Possible interactions between EGFR vIII mediated regulation of proliferation and metabolism in glioma cells.

Gisle Størseth Solhaug

Master thesis, Pharmacy

Centre for Pharmacy / Department of Biomedicine
University of Bergen
2009

1. Acknowledgments

This work was carried out at the Department of Biomedicine, University of Bergen, from 4th August 2008 until 20th May 2009.

First I would like thank my supervisor associate Professor Karl Johan Tronstad for always helping me out and offering valuable advice.
Next, I am very grateful to my co-supervisor Hanne R. Hagland for answering my never-ending questions and for bearing all additional work I have put her through. I will also like to thank my fellow student, Ingunn Bergslien, for great collaboration and enjoyable lunch breaks.
My thanks also go to my remaining lab-group, Julie Nikolaisen, Ingrid Strand and Linn H. Nilsson for all help and support and for creating a great work environment.

Finally, I would like to thank girlfriend Nhung, my family and my friends for all support and encouragement.

Bergen, 19th May 2009

Gisle Størseth Solhaug

2. Table of contents

3. Abbreviations

Abbreviation	Full name
ALD	Fructose bisphosphate aldolase
AMPK	AMP-activated protein kinase
AR	Amphiregulin
ATP	Adenosine triphosphate
BrdU	Bromodeoxyuridine
BSA	Bovine serum albumine
BTC	Betacellulin
CoA	Coenzyme A
CTMP	Carboxy terminal modulating protein
DCFH	Dichloro fluorescein
DMEM	Dulbecco's modified eagle's medium
DMSO	Dimetyl sulfoxide
EDTA	ethylenediaminetetraacetic acid
EGFR	Epidermal growth factor receptor
ELISA	Enzyme-linked immunosorbent assay
ENO	Enolase
EPR	Epiregulin
ERK	Extracellular signal-regulated kinases
ETC	Electron transport chain
FACS	Fluorescence-activated cell sorting
FAD	Flavin adenine dinucleotide
FBS	Foetal bovine serum
FCCP	Carbonyl cyanide-p-trifluoromethoxyphenylhydrazone
FdG	Fluorodeoxyglucose
FH	Fumarate hydratase
FSC	Forward scatter
G6P	Glucose 6-phosphate
GAPDH	Glyceraldehyde 3-phosphate dehydrogenase
GBM	Glioblastoma multiforme
GLUT	Glucose transporter
GPI	Glucose phosphate isomerase
Grb2	Growth factor receptor-bound protein 2

HB-EGF	Heparin-binding epidermal growth factor
HIF	Hypoxia inducible factor
HK	Hexokinase
IMM	Inner mitochondrial membrane
IMS	Inter membrane space
JAK	Janus kinase
LDH	Lactate dehydrogenase
m2-PK	pyruvate kinase M2
MAPK	Mitogen-activated protein kinase
mDNA	Mitochondrial DNA
MEK	MAPK/ERK kinase
MRDR	Mito tracker deep red
mTOR	Mamalian target of rapamycin
MTT	3-(4,5-dimethylthiazol-2-yl)-2,5-diphenyltetrazolium bromide
NAD	Nicotinamide adenine dinucleotide
NaDOC	Sodium deoxylate
NAO	Nonyl acridine orange
NO	Nitrogen oxide
OMM	Outer mitochondrial membrane
PDK1	PIP3-dependent kinase 1
PET	Positron-emission tomography
PFK	Phosphofructo kinase
PGK	Phosphoglycerate kinase
PGM	Phosphoglycerate mutase
PH	Pleckstrin homology
PI3K	Phosphoinositide 3-kinase
PIP_2	Phosphatidylinositol 3,4 -bisphosphate
PIP_3	Phosphphatidyl-inositol 3,4,5- bisphosphate
PK	Pyrovate kinase
PTEN	Phosphatase and tensin homologue deleted on chromosome 10
PYK	Pyruvate kinase
rictor	Rapamycin – insensitive companion of mTOR
ROS	Reactive oxygen species
Rsk	Ribosomal S6 protein kinase

RTK	Tyrosine kinase receptors
SDH	Succinate dehydrogenase
SDS-PAGE	Sodium dodecyl sulphate polyacrylamide gel electrophoresis
SHIP	SH2-containing inositol phosphatase
SOS	Son of sevenless
SSC	Side scatter
STAT	Signal transducers and activator of transcription
TGF-α	Transforming growth factor α
TMRM	Tetramethyl rhodamine methyl ester
TPI	Triosephosphate isomerase
tRNA	Transfer RNA
UCP	Uncoupling protein
VDAC	Voltage-dependent anion channel
VHL	Von Hippel-Lindau protein
WT	Wild type

4. Introduction

4.1 Cancer

The life cycle of a normal cell is strictly controlled by multiple check points and regulatory factors. Cancer cells on the other hand contain defects in the regulatory machinery that govern cell proliferation and homeostasis, which in turn may lead to tumor formation [1]. For the majority of cancer cells a number of characteristic features seem to contribute to the tumor development. These physiological changes include; insensibility to growth-inhibitory signals, inhibition of programmed cell death, self-sufficiency in growth signals, sustained angiogenesis, limitless replicative potential and tissue invasion and metastasis [1]. In addition to uncontrolled cell proliferation, most tumors are also characterized by specific changes in energy metabolism. Tumor cells tend to take up large amounts of glucose and secrete lactate. The fact that cancer cells may generate many of their needed growth signals reduces their dependence of stimuli from other tissues [1] . Some of these signals can be sensed by the epidermal growth factor receptor (EGFR) and may contribute in the regulation of tumor cell metabolism and proliferation.

4.2 Glucose catabolism and cellular bioenergetics

4.2.1 Glycolysis

Glycolysis is the process where glucose is transformed into 2 molecules of pyruvate in order to be utilized for energy production. This pathway contains 10 enzymatic steps and takes place in the cytosol [2]. The glycolysis is divided into two phases (Figure 4.1). In the preparatory phase 2 molecules of adenosine triphosphate (ATP) are invested to raise the free energy state within the adapted glucose molecule. This energy gain is used for the production of 2 nicotinamide adenine dinucleotide (NADH) and 4 ATP molecules in the payoff phase. The overall equation of glycolysis is:

$$\text{Glucose} + 2\ NAD^+ + 2\ ADP + 2P_i \rightarrow 2\ \text{pyruvate} + 2\ NADH + 2H^+ + 2\ ATP + 2\ H_2O$$

The further fission of pyruvate is normally determined by the oxygen level. If oxygen is absent (anaerobic conditions) pyruvate is reduced to lactate in a process catalyzed by lactate dehydrogenase (LDH). Under aerobic conditions (oxygen present) pyruvate are translocated into mitochondria and completely oxidized to CO_2 and H_2O, and the reduction of pyruvate to lactate is prevented. Findings by Pasteur showed an elevated use of glucose when oxygen

were absent compared to aerobic conditions, and this phenomenon has been named the Pasteur effect [3].

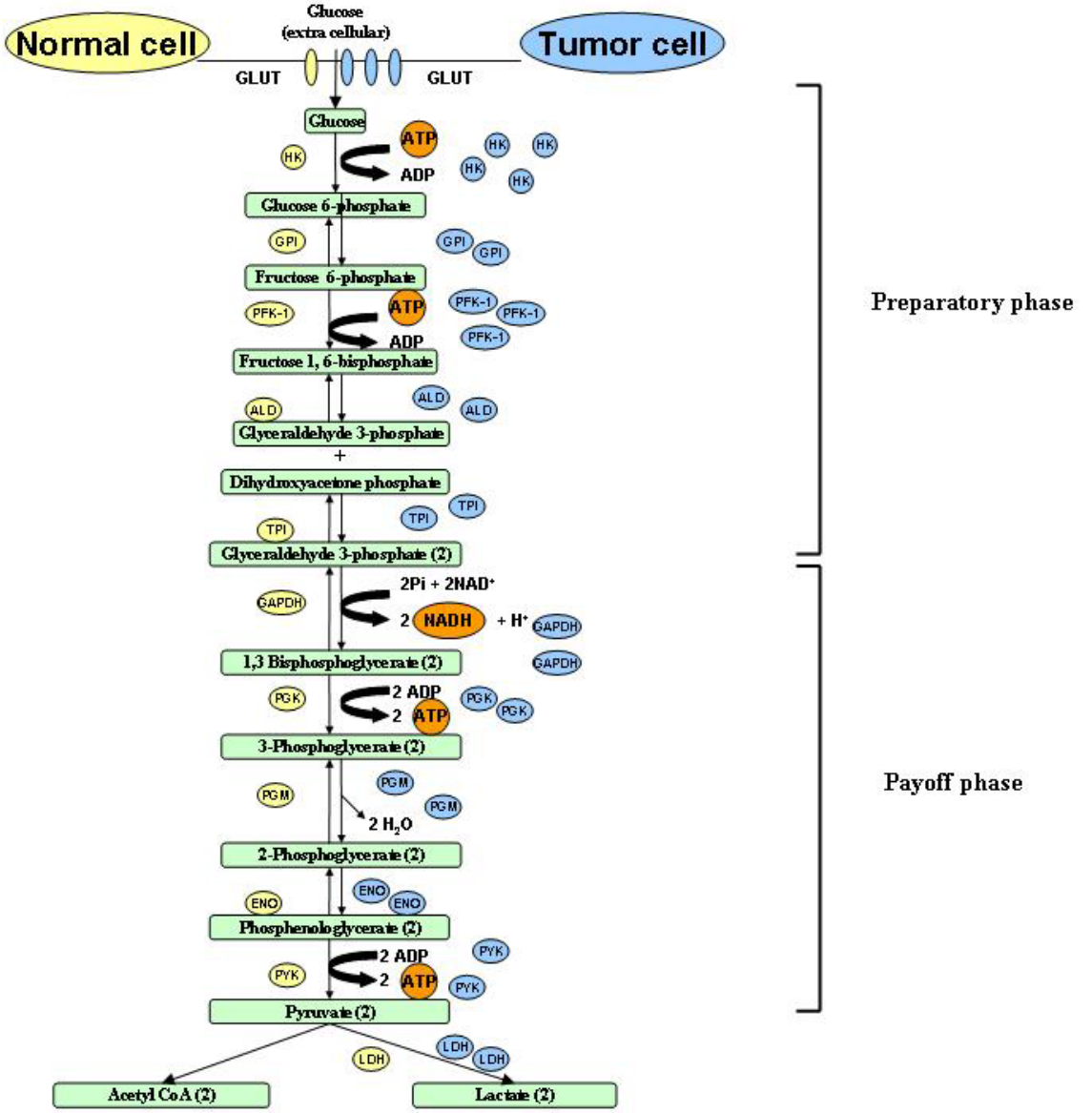

Figure 4.1. The glycolytic pathway in normal (left) versus malign cells (right). The glucose molecules are unable to diffuse through the plasma membrane, and therefore depend on glucose transporters (GLUTs) to enter the cell. Once in the cytosol, glucose enters the glycolytic pathway and is converted to pyruvate. (Alternatively, at rest periods glucose enters the glycogenesis where it is converted to glycogen for long time storage).
Malign cells tend to have a modified metabolism, and the most notorious alteration of energy metabolism is an elevated glycolytic capacity [4]. This is obtained by overexpression of glycolytic enzymes and transporters as illustrated in this figure. The yellow spheres represent levels of enzymes/transporters in healthy cells, while blue spheres represent tumor cells conditions. Here, GLUT = glucose transporter, HK = hexokinase, GPI = glucose phosphate isomerase, PFK-1 = phospho fructokinase-1, ALD = fructose bisphosphate aldolase, TPI = triosephosphate isomerase, GAPDH = glyceraldehyde phosphate dehydrogenase, PGK = phosphoglycerate kinase, PGM = phosphoglycerate mutase, ENO = enolase, PYK = pyruvate kinase , LDH = lactate dehydrogenase [4].

4.2.2 Mitochondrial ATP synthesis

The mitochondria are known as the cellular power plants and are the home of the citric acid and electron transport chain (ETC). Central elements of mitochondrial structure and function are described in Figure 4.2.

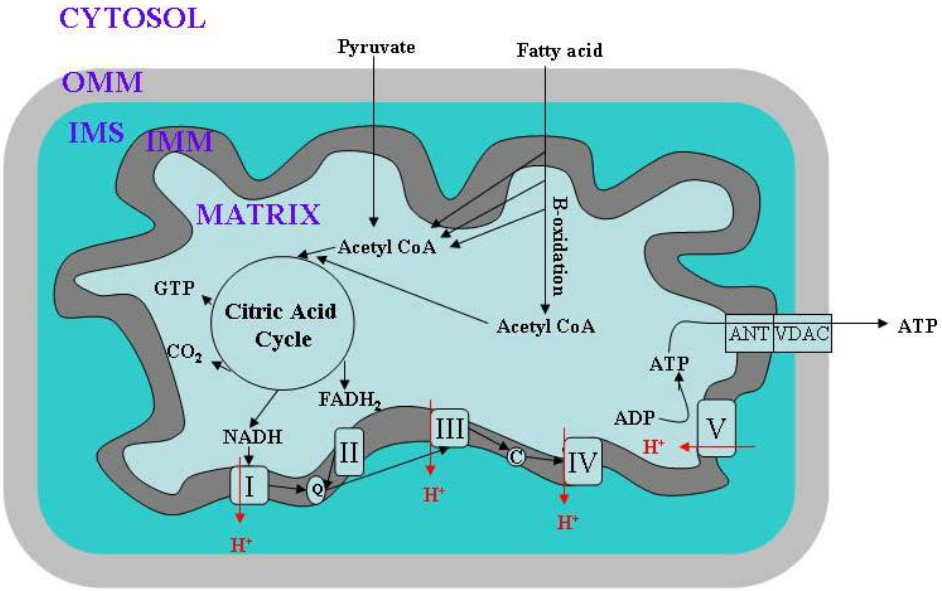

Figure 4.2 Mitochondrial structure and function. The mitochondrial matrix is enclosed by two lipid membranes, an outer mitochondrial membrane (OMM) and an inner mitochondrial membrane (IMM). The pocket between the membranes is known as the inter membrane space (IMS). The IMM is folded by invaginations called cristae, which gains a greater surface area. The citric acid cycle is located in the matrix, while the ETC is located in the inner mitochondrial membrane.

Mitochondria contain small circular DNA molecules referred to as the mitochondrial genome. The 16,6 kb mitochondrial DNA (mtDNA) is responsible for encoding 13 of the proteins found in the ETC, but also 2 rRNAs and 22 tRNAs necessary for mitochondrial gene translation. In addition the genome contains a non coding region called the D-loop [5]. Mitochondrial proteins involved in replication, transcription and translation are under control by nuclear DNA. The D-loop region of the mtDNA has been termed "the mutational hot spot" and mutations in this region have been found in most examined tumors [6]. As mammalian mtDNA lack histones and introns it is tenfold more vulnerable to mutations and oxidative damage than nuclear DNA [7].

4.2.2.1 Citric acid cycle

Before entering the citric acid cycle the pyruvate produced during glycolysis is irreversible oxidized to acetyl CoA. This is a key molecule in the energy metabolism also being the end product yielded by fatty acid- and amino acid degradation. Acetyl CoA enters the citric acid cycle and is converted to oxaloacetate through eight sequential reactions (Figure 4.3). The total energetic outcome from one acetyl CoA molecule oxidized by the cycle is 1 $FADH_2$, 1 GTP (equivalent to 1 ATP) and 3 NADH.

Recent discoveries of mutations in the nuclear genes of the citric acid cycle enzymes succinate dehydrogenase (SDH) and fumarate hydratase (FH) has provided proof that primary inherited abnormalities in mitochondria can cause tumors [8].

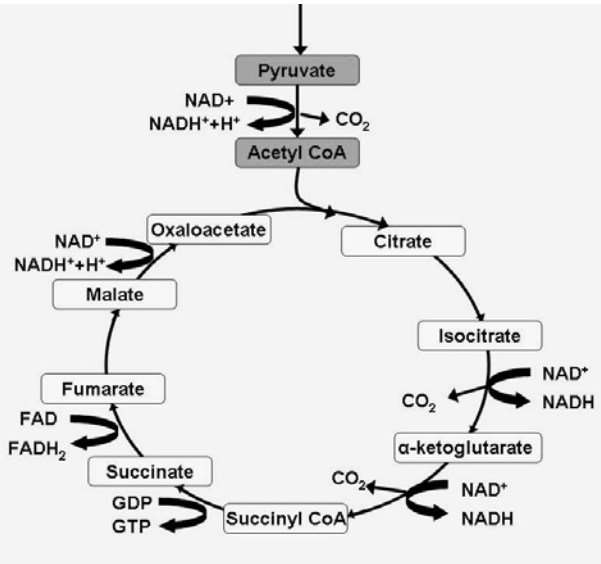

Figure 4.3 Overview of the citric acid cycle.

4.2.3 Mitochondrial respiration – oxidative phosphorylation

The ETC is located in the cristae of the inner mitochondrial membrane and contain 4 protein complexes (Complex I - IV) that are linked together by the electron transporters coenzyme Q and cytochrome c (Figure 4.4). The ETC is the terminal step of the energy metabolism and here the remaining energy of oxidized nutrients are used to drive the synthesis of ATP via ATP synthase (complex V).

Electrons are loaded into the chain by the electron transporters NADH and $FADH_2$. NADH donates electrons to complex I (NADH dehydrogenase) and $FADH_2$ to complex II (succinate dehydrogenase). The electrons are transferred stepwise between the complexes and finally donated to molecular oxygen at complex IV (cytochrome oxidase enzyme), forming 2 molecules of water. As the electrons move through the chain, protons are simultaneously translocated from the matrix to the IMS. The proton release leads to an increased proton gradient across the IMM, making the matrix negatively charged. These factors are collectively termed the proton motive force. This mitochondrial membrane potential ($\Delta\Psi m$) is a hallmark of respiratory function and is often modified in malign cells [9]. Further, the proton motive force drives the movement of protons into the mitochondrial matrix through Complex V. As the protons cross the IMM their free energy is donated and used for the synthesis of ATP from ADP and Pi. The synthesised ATP is transported out of the mitochondria through ANT/VDAC channels [10].

Uncoupling is the process when the link between proton motive force and ATP synthesis is broken and protons freely leak through the IMM. Under such conditions energy is released as

heat instead of being utilized for ATP production. Uncoupling is a natural occurring event carried out by uncoupling proteins (UCPs), but can also be initiated by chemical uncouplers such as carbonyl cyanide-p-trifluoromethoxyphenylhydrazone (FCCP) [11].

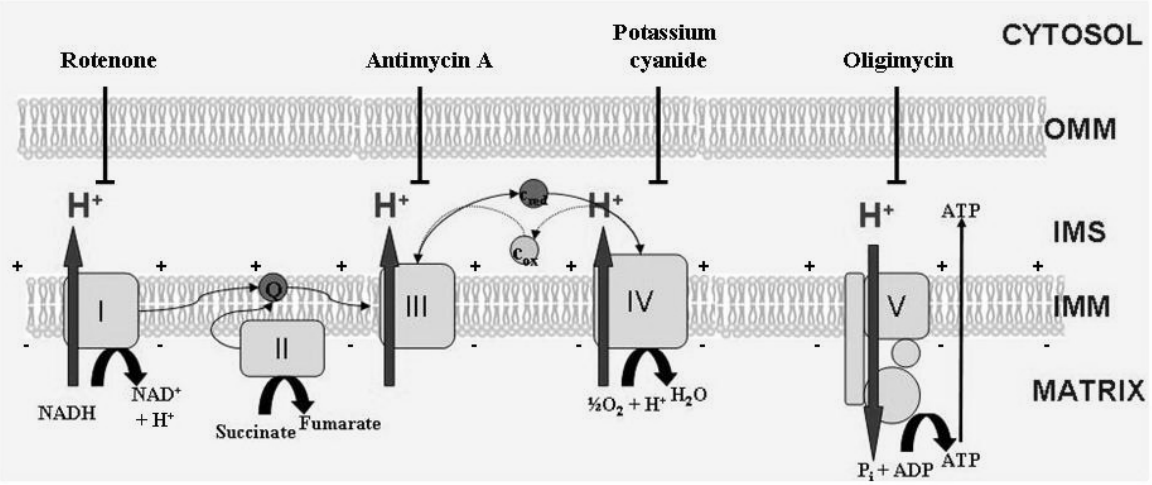

Figure 4.4. The electron transport chain. The figure presents the movement of electrons between the different complexes and the formation of a proton gradient used for ATP synthesis (see text for further details). Inhibitors of the different ETC complexes are shown at the top.

The ETC is associated with the production of reactive oxygen species (ROS). Under stressful conditions an elevated ROS production may occur, leading to damage of cellular compounds [12]. ROS can also influence mitochondrial function, thus lowering the respiratory energy production.

A modified metabolic status can be sensed by AMP-activated protein kinase (AMPK) [13] which may alter the mitochondrial biogenesis through elevated expression of mitochondrial proteins and enhanced mitochondrial proliferation. ROS production and mitochondrial mass are measurable properties that can be impaired in tumor cells.

4.3 Tumor cell metabolism

4.3.1 Warburg effect

Normal cells have a finely tuned balance between glycolysis and oxidative phosphorylation for ATP production. In most malign cells this balance is disrupted with an increased glycolytic activity and a down regulation of the mitochondrial respiration even in the presence of oxygen (aerobic glycolysis) [14]. Under such conditions pyruvate is reduced to lactate with the excess lactate being excreted from the cell. These findings were observed by Otto Heinrich Warburg back in 1924, and have later been termed the “Warburg effect”. Warburg postulated that these changes in metabolism were the fundamental cause of cancer [15].

Today, more than 8 decades later, the mutation in tumor suppressor genes and oncogenes are known to be the fundamental triggers in carcinoma development [16]. There are several hypotheses why the "Warburg effect" occurs in tumor cells; i) it may be an adaption to the low-oxygen environment that can be found in tumors, ii) a result of cancer genes shutting down the mitochondria because of their contribution in the apoptotic program or iii) simply because the mitochondria are damaged in cancer [4].
The fact that most primary and metastatic human cancers have a high uptake and consumption of glucose can be used in clinical application. The utilization of the glucose analogue tracer fluorodeoxyglucose (FdG) in positron-emission tomography (PET) gains sensitive information of tumor development [17].

In contrast to normal cells an overexpression of glycolytic enzymes and glucose transporters are often found in malignant cells. The increased glycolytic flux has been proposed to be a metabolic strategy of tumor cells to ensure survival and growth when facing hypoxic conditions[14].

4.3.2 HIF-1 – A trigger of glycolytic abnormalities

Activation of hypoxia inducible factor-1 (HIF-1) is believed to be a main mechanism triggering the enhanced glycolysis in tumor cells [4]. Being a transcription factor for glycogenic genes, HIF-1 promotes the expression of the enzymes hexokinase (HK), phosphofructokinase 1 and 2 (PFK-1, PFK-2), aldehyde dehydrogenase (ALD), glyceraldehyde 3-phosphate dehydrogenase (GAPDH), phosphoglycerate kinase (PGK), enolase (ENO), pyruvate kinase (PYK) and lactate dehydrogenase (LDH) (Figure 4.1). All together this stimulates the glycolytic flux [18, 19].
HIF-1 consists of the two subunits HIF-1α and HIF-1β where the α-subunit determines the stability of the complex. At aerobic conditions HIF-1α is actively led to degradation by the von Hippel-Lindau protein (VHL) at the proteasome, while in lack of oxygen HIF-1α becomes highly stable. At aerobic conditions HIF-1α may be induced by growth factors (EGFR), ROS (reactive oxygen species), NO (nitrogen oxide) and cytokines [20, 21]. Mutations in the von Hippel-Lindau protein have been found in some aggressive tumors leading to an enhanced HIF-1 concentration [21].

4.3.3 Glycolytic enzymes and transporters

Tumor cells depend on their ability to survive under stressful and variable conditions. In fast growing tumors hypoxic areas with limited blood supply are often seen, and here the level of glucose, oxygen and other substrates may be low [4].

The enhanced glycolytic activity within tumor cells is believed to occur due to the increased expression of glycolytic enzymes and transporters [14]. A large number of studies have shown that the protein isoforms hexokinase II (HK-II), GLUT-1, phosphoglucomutase (PGM), pyruvate kinase M2 (m2-PK), lactate dehydrogenase-A and isoforms of the lactate transporter are frequently overexpressed in multiple cancers [4].

4.3.3.1 Hexokinase

Hexokinase (HK) is the first enzyme in the glycolytic pathway and is responsible for the transformation of glucose to glucose 6-phosphate (G6P) (Figure 4.1). Four different isoforms of HK are found in mammalian cells, named HK-I to HK-IV [22] . The isoforms differ in kinetic properties and have tissue specific localization. HK-II has shown to be the predominant isoform in fast growing tumor cells, except from brain tumors where HK-I is overexpressed [23].

HK-II is able to bind to the outer mitochondrial membrane through a specific interaction with the voltage-dependent anion channel (VDAC). This protects the kinase from degrading proteases and enables to give a direct access to the newly synthesized ATP from ATP synthase [24]. Studies indicate that the HK-II - VDAC complex formation may interfere with the function of the pro-apoptotic protein Bax. When binding VDAC, Bax is responsible for the release of cytocrome c and other apoptotic mitochondrial proteins under stress conditions [25]. Therefore HK-II may have an additional role as an inhibitor of apoptosis.

The accumulation of a product may decrease the further reaction through a negative control mechanism. This effect is seen in the glycolysis with G6P being a potent inhibitor of HK-I, HK-II and HK-III [22]. The binding of HK to the mitochondria was therefore believed to be a mechanism to bypass the G6P inhibition.

4.3.3.2 GLUT

Glucose molecules lack the ability to diffuse through the cellular membrane and depend on ATP-driven transporters to enter the cytoplasm (Figure 4.1). This transport is carried out by trans-membrane glucose transporters (GLUTs), a family of proteins consisting of at least 13 members [26]. In order to utilize the increased glycolytic capacity for energy production, malignant tissues depend on an enhanced income of glucose. Mutations in the genome leading

to overexpression of the GLUTs are found in a variety of cancers and is considered to be critical for tumor maintenance [14]. Studies indicate that the tumor GLUT activity is 10-12 folds higher compared to non-tumorigenic cells (Figure 4.1) [27].

4.3 EGFR structure and function

The epidermal growth factor receptor (EGFR) is located at the cell surface and is activated when binding its ligand epidermal growth factor (EGF) (Figure 4.5). EGFR belongs of the ErbB family of tyrosine kinase receptors (RTK) which consists of four members; EGFR (ErbB-1), ErbB-2, ErbB-3 and ErbB-4. All these proteins have an extracellular ligand binding site, a hydrophobic trans-membrane domain and an intracellular domain containing tyrosine kinase activity. The main difference is found in the extracellular domain where the four receptors show a different ligand binding specificity [28].

The EGFR binding ligands can be divided into two groups; i) EGFR specific ligands that include EGF, transforming growth factor α (TGF-α) and amphiregulin (AR). ii) Ligands with a dual specificy for both EGFR and ErbB-2 receptors. This group include heparin-binding growth factor (HB-EGF), betacellulin (BTC) and epiregulin (EPR) [29].
The ErbB receptors ligands may be secreted either by the receptor containing cell itself (autocrine secretion) or by surrounding cells (paracrine secretion) [28].

When binding their ligands the ErbB receptors may form homo-dimers by cross binding to a similar protein or hetero-dimers by linking to a different receptor of the ErbB family. After dimerization the receptors are often endocytosed and linked to the adaptor protein, c-cbl, which targets it for degradation. This regulatory process helps limiting the signalling outcome of the ligand binding [30, 31].

4.4 EGFR signalling –Down stream effects

A variety of downstream proteins may be activated upon binding of EGF to its receptor. EGFR takes part in a multiple cellular events and is known to trigger the three well known pathways; i) Ras-Raf-MEK-ERK-pathway, ii) PI3 kinase/Akt-pathway and iii) JAK/STAT-pathway [32] (Figure 4.5). The PI3 kinase/Akt pathway has been proven to be an important regulator of metabolism and glycolysis in cancer cells [33] and is of particular interest for the presented project.

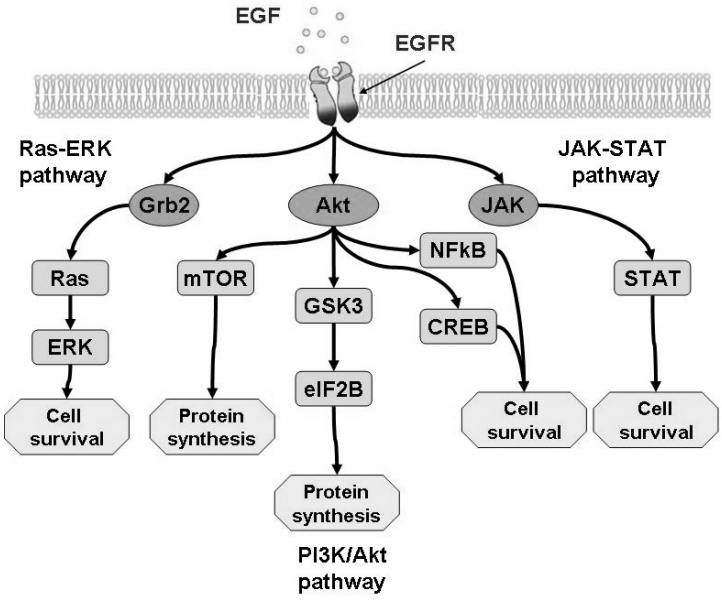

Figure 4.5. The downstream effects of EGFR activation.

4.4.1 PI3 kinase/Akt-pathway

The Akt signalling pathway may be engaged by receptor tyrosine kinases such as EGFR. Akt is a threonine-serine kinase and is a member of the "cAMP-dependent, cGMP-dependent protein kinase C"- family of kinases [34]. The protein consist of three isoforms; Akt1, Akt2 and Akt3, and all contain a N-terminal pleckstrin homology (PH) domain and a C-terminal kinase domain [35]. Akt is a well known pro survival factor, and downstream of the protein a branched network of more than 3000 substrates has been identified. Akt is in part responsible for the increased resistance to apoptosis, the uncontrolled cell proliferation and the altered cell metabolism which are characteristic features of transformed cells [36]. Additionally Akt has been shown to be involved in cellular processes as transcription, translation, cell growth and angiogenesis (Figure 4.6) [37]. Akt also positively regulate the activity of the protein synthesis regulator mammalian target of rapamycin (mTOR) [38].

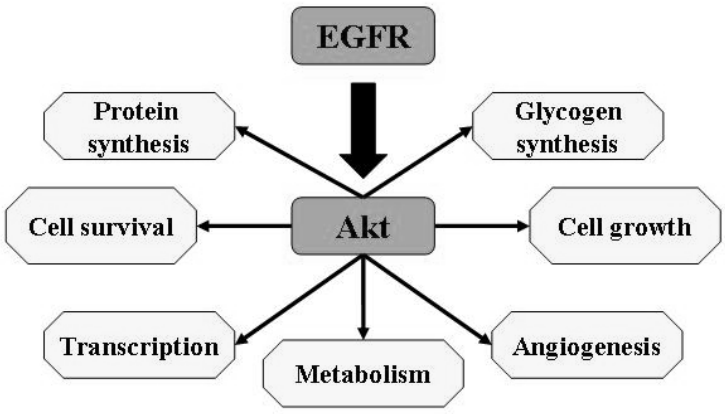

Figure 4.6. The multiple roles of Akt in cellular responses.

Upon activation, EGFR attracts the lipid kinase phosphoinositide 3-kinase (PI3K). PI3K consist of two subunits that must be linked together to yield an active form. As mentioned earlier the growth receptor contains a phosphorilated tyrosine (Y) residue that may serve as a docking site, this time for the PI3K p85 subunit. Once bound the p110 subunit is recruited to the complex. When activated, PI3K phosphorylate inositol ring 3'OH groups in phosphatidylinositol 3,4 -bisphosphate (PIP_2) and adds an inositol group to the molecule forming phosphphatidyl-inositol 3,4,5- bisphosphate (PIP_3) [39]. PIP3 recruit a diversity of signalling proteins with PH domains to the plasma membrane where they are activated [40]. Among these proteins are PDK1 (PIP3-dependent kinase 1) and Akt. The binding of Akt to PIP3 is thought to provoke conformational changes in Akt, resulting in the exposure of its two main phosphorylation sites Thr 308 and Ser 473. Akt is then phosphorylated by PDK1 and the mTOR/rictor-complex [41].

An important negative regulator of the PI3K/Akt pathway is the lipid phosphatase phosphatase and tensin homologue deleted on chromosome 10 (PTEN). This enzyme reverses the process by removing the 3-phosphate from PIP_3 to produce PIP_2. In certain cancers the gene encoding PTEN may be mutated, giving a decreased PTEN function. As a consequence the level of PIP3 rises, leading to an increased Akt activation [42]. Additional negative regulators are the phosphatase SH2-containing inositol phosphatase (SHIP) and the newly discovered carboxy terminal modulating protein (CTMP). The importance of SHIP and CTMP in PI3K-Akt regulation is unclear since there have been no reports of altered levels in human cancers [43].

4.4.2 AMPK

AMP-activated protein kinase (AMPK) is a protein system acting as a sensor of cellular energy, a system found within all genetic determined eukaryotic cells [13]. The protein complex is activated by an increase in the cellular AMP/ATP ratio that occurs due to metabolic stresses that accelerate ATP consumption or interfering with the ATP production [13] . When activated, AMPK initiates catabolic processes responsible for ATP production and turns of ATP-consuming pathways (proliferation and cell growth) through modulation of multiple down-stream proteins [13]. As seen in figure 4.7 AMPK takes part in down-regulation of protein synthesis and up-regulating of fatty acid oxidation. AMPK is also an up-stream activator of the p53 stress sensor [44].

AMPK is a heterotrimer consisting of the three subunits α, β and γ. The α-subunit has catalytic activity, and the β subunit contains a glycogen binding site while the γ-subunit binds

the inhibitory ATP or the activating AMP at two regulatory sites [13]. Binding of AMP to AMPK causes an allosteric change that activates the complex and also promotes further phosphorylation of the AMPK α-subunit by the kinase LKB1. This phosphorylation is necessary for the full activation of AMPK [45].

In cancer cells, the rapid growth and disordered angiogenesis can create hypoxic areas with limited nutrition supply. Under such stressful conditions AMPK can be activated. Recent studies have shown that AMPK control mechanisms contribute in the regulation of apoptosis and growth in tumor cells[46] .Paradoxically, AMPK activation has been suggested to be necessary for tumor cell survival and expansion, at least in the short turn by preventing further cell growth before nutrients are supplied by raised angiogenesis [47].

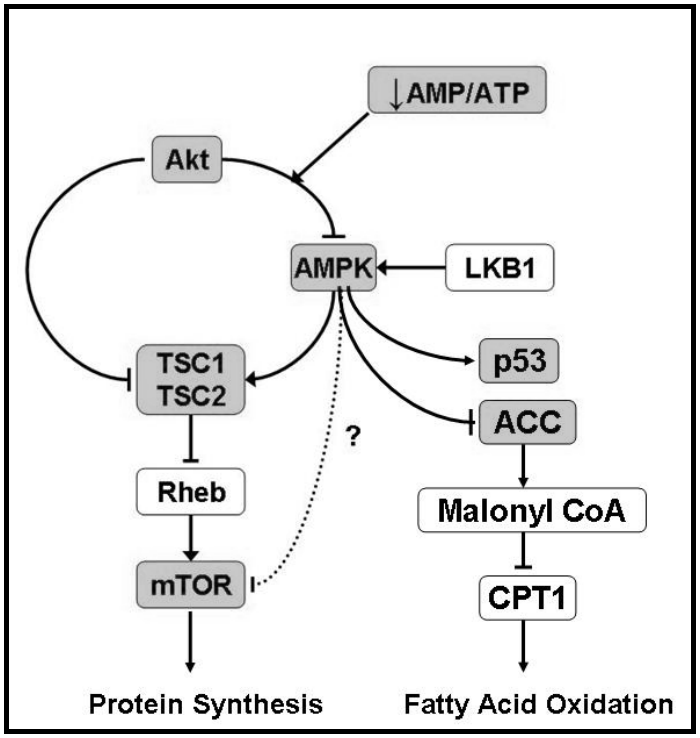

Figure 4.7 AMPK regulation. Akt activation of mTOR is believed to be regulated by Akt through at least two distinct pathways. Akt is capable of activating mTOR direct by phosphorylation and inhibition of the negative mTOR regulator tuberous sclerosis complex 2 (TSC2) and Rheb. Recent data has shown an additional pathway in which Akt regulates mTOR activation, namely through inhibition of the TSC2 activator AMPK. By stimulating ATP production, Akt decreases the AMP/ATP ratio and therefore reduces AMPK activity [38]. It has been suggested that AMPK can directly phosphorylate and inactivate mTOR, but this has not yet been verified [48]. AMPK binding of AMP also facilitates phosphorylation of Thr 172 by LKB1, and this further enhances enzyme activity [45]. AMPK is an upstream regulator of acetyl-CoA carboxylase (ACC) and is therefore capable of upregulating the fatty acid oxidation. Activated AMPK has proven to be an initiator of the stress signal p53 [44].

4.5 Alternative EGFR modulated metabolic regulators

The link between the tumor suppressor p53 and cancer development and progression is well established [49]. During the last years the role of p53 has emerged, being an important metabolic regulator of both the glycolytic and mitochondrial respiratory pathways. p53 has been shown to be involved in upregulation of HK and having an inhibitory effect on PFK-1 and PGM in the glycolysis [50-52]. Studies have shown that p53 is able to promote the aerobic respiration by an increased expression of Complex IV subunits in the ETC [53] and to affect the glucose uptake by binding GLUT1 and GLUT4 [54].

The signalling pathways Ras-Raf-MEK-ERK and JAK/STAT may also take part in EGFR mediated metabolic regulation through their controlled expression of various genes [55, 56].

5. Aims

Tumor cells tend to have a manipulated energy metabolism, presented by an elevated glycolytic activity and decreased mitochondrial respiration. This behaviour can be caused by several factors such as oncogene signalling, hypoxia, mitochondrial dysfunction or over-expression of metabolic enzymes and proteins.

The objective of the presented study was to determine if EGFR represents a possible regulatory link between cellular proliferation and energy metabolism in cancer cells.

In this study two different U87 glioblastoma cells were studied; a wild type cell line and a mutated cell line expressing the constitutively active EGFR vIII protein. By measuring multiple cellular- and mitochondrial properties we also wanted to examine if the mitochondria play different roles within the two samples. The following aims can be highlighted;

1. Determine if altered EGFR signalling affects cell proliferation.
2. Investigate if EGFR vIII expression changes energy metabolism within cancer cells.
3. Examine if pharmacological manipulation of the metabolism can change the growth potential of the cancer cells. If this is the case, may EGFR vIII involved?
4. Investigate possible interactions between EGFR with major signalling factors such as Akt and AMPK.

6. Materials

6.1 Chemicals

Chemicals	Abbreviation/ Chemical formula	MW, g/mol	Supplier
2-deoxy-D-glukose	$C_6H_{12}O_5$	164,16	Sigma
2-Mercaptoethanol	$C_2H_{12}OS$	78,1	Merck
30 % akrylamid/bis solution, 37,5:1	-	-	Merck
Ammonium persulphate	APS, $H_8N_2O_8S_2$	228,2	BioRad
Aprotinin from bovine lung	$C_{284}H_{432}N_{84}O_{79}S_7$	6511,44	Sigma
Bovine serum albumin, 1,49mg/ml	BSA	-	Sigma-Aldrich
Carbonyl cyanide 4-(trifluormetoksy)-phenylhydrazone	FCCP , $C_{10}H_5F_3N_{40}$,	254,17	Sigma
Cytocrome c	Cyt c	12500	Sigma
Digitonin, ~50% (TLC)	$C_{56}H_{92}O_{29}$	1229,31	Fluka
Dimethyl sulphoxide	DMSO, $(CH_3)_2SO$	78,1	Merck
Disodium hydrogen phosphate	Na_2HPO_4	141,96	Sigma
Dimetylsulfoxid HYBRI-MAX®	DMSO, $(CH_3)_2SO_4$	78,1	Sigma
Dulbecco's Modified Eagle's Medium (+ 4500 mg glucose/L, without L-glutamin)	DMEM	-	Sigma
Dulbecco's Modified Eagle's Medium without phenol red (+ 4500 mg glucose/L, with L-glutamin)	DMEM	-	Gibco
Ethanol, 96%	C_2H_5OH	46,1	Vinmonopolet
Ethylene glycol tetraacetic acid	EGTA	380,4	Sigma
Foetal bovine serum	FBS	-	PAA: The Cell Culture Company
Formaldehyde, 37% solution	CH2O	30,03	Sigma
Freeze dried milk (0,6% fat)	Mlk	-	Marvel
Glutamate	$C_5H_8NO_4Na$	169,1	Sigma
Glycine, > 99,7 %	$C_2H_5NO_2$	75,07	Merck
Glycerol > 99,5%	$C_3H_8O_3$	92,1	Fluka
HEPES	$C_8H_{18}N_2O_4S$	238,3	Sigma
Hydrocloric acid	HCl	36,5	Merck
Hydrogen peroxide solution, 30% in H_2O	H_2O_2	34,01	Sigma
Hydrazine	$H_2NNH_2{\cdot}H_2O$	32,04	Sigma
K-lactobionate	$C_{12}H_{22}O_{12}$	358,3	Fluka
Leupeptin hemisulphate salt	$C_{20}H_{38}N_6O_4{\cdot}\ 1/2H_2SO_4$	475,59	Sigma

Luminol, >97 %	$C_8H_7N_3O_2$	177,16	Sigma
L-glutamine	$C_5H_{10}N_2O_3$	146,14	Sigma
Magnesium chloride	$MgCl_2 \cdot 6H_2O$	203,3	Scharlau
Malic acid	C4H6O5	134,1	Sigma
Methanol	CH_3OH	32,0	Merck
Monopotassium phosphate	KH_2PO_4	136,1	Merck
NAD^+	-	663,43	Fluka
N,N,N',N'-tetrametyletylendiamid	$C_6H_{16}N_2$, TEMED	116,2	BioRad
Nonidet P40	NP40, $(C_6H_4O)_nC_{14}H_{22}O$	-	Sigma
Oligomycine	-	800	Sigma
p-Coumaric acid	$HOC_6H_4CH=CHCO_2H$	164,16	Sigma
Penicillin/Streptomycin (100x)	PenStrep, $C_{16}H_{17}N_2NaOS:C_{42}H_{84}N_{14}O_{26}S_3$	-	PAA: The Cell Culture Company
Phenylmetanesylphonyl fluoride	PMSF, $C_7H_7FO_2S$	174,19	Sigma
Ponceau S	$C_{22}H_{12}N_4Na_4O_{13}S_4$	760,57	Sigma
Rotenone	$C_{23}H_{22}O_6$	394,42	Sigma
Sodium chloride	NaCl	58,44	Merck
Sodium deoksycholate	NaDOC,C24H39O4· Na	414,6	Calbiochem
Sodium orthovandat	Na3VO4	183,91	Sigma
Sodium dodecylsulphate	SDS, $C_{12}H_{25}O_4SNa$	288,4	Merck
Sucrose	$C_{12}H_{22}O_{11}$	342,3	Roth
Taurine	$C_2H_7NO_3S$	125,1	Sigma
Trizma® base, >99,9 % titrering	TRIS, $C_4H_{11}NO_3$	121,14	Sigma
Trypan Blue	$C_{23}H_{24}N_6O_{14}S_4Na_4$	960,81	Sigma
TWEEN® 20	-	-	Sigma

6.2 Solutions and buffers

6.2.1 Standard culture medium

Solution	Ingredients	Final concentration
DMEM medium	DMEM with 4,5g/L glucose, without L-Glutamine	89 % (v/v)
	Foetal Bovine Serum*	9 % (v/v)
	L-glutamine	1 % (v/v)
	Penicillin/Streptomycin (100x)	1 % (v/v)

* Heat inactivated for 30 minutes at 56^{o}C

6.2.2 PBS solution

Solution	Ingredients	Final concentration
PBS x1	NaCl	8 g
	KCl	0,2g
	Na_2HPO_4 x H_2O	2g
	KH_2PO_4	0,4g
	H_20	To 1 litre
	NaOH	To pH 7,3

6.2.3 Cryogenic medium

Solution	Ingredients	Final concentration
Cryogenic medium	DMEM with 4,5g/L glucose, without L-glutamine	70 % (v/v)
	Foetal bovine serum (FBS)	20 % (v/v)
	DMSO (Dimetyl sulfoxide 200mg/ml)	10 % (v/v)

6.2.4 Buffers for cell lysation

Solution	Ingredients	Final concentration
NP40-RIPA buffer	NP40 (Nonidet P40)	1 % (v/v)
	10% SDS	1 % (v/v)
	NaDOC (Sodium deoxylate)	0,5 % (w/v)
	1M TRIS, pH 7,4	5 % (v/v)
	5M NaCl	3 % (v/v)
	H_2O	87 % (v/v)
RIPA buffer*	Aprotinin 1µg/µl	0,1 % (v/v)
	Leupeptin 1µg/µl	0,1 % (v/v)
	Natrium Vanadat 100µM	1,0 % (v/v)
	PMSF (phenylmethylsulponylfluoride)	1,0 % (v/v)
	NP40-RIPA buffer	97,8 % (v/v)

*Must be freshly made since the PMSF is only active for 30 minutes after the mix of the reagents.

6.2.5 Gels and solutions for SDS-PAGE and Western Blotting

Solution	Ingredients	Final concentration
10% Separating gel	30% Acrylamide/bis solution	10 % (w/v)
	1,5mM TRIS pH 8,8	375mM
	H_2O	40,5 % (v/v)
	SDS 10%	0,1 % (w/v)
	Ammonium persulphate 10%	0,05 % (w/v)
	TEMED	0,05 % (w/v)
4% Stacking gel	30% Acrylamide/bis solution	4 % (w/v)
	0,5mM TRIS pH 6,8	125mM
	H_2O	60 % (v/v)
	SDS 10%	0,1 % (w/v)
	Ammonium persulphate 10%	0,05 % (w/v)
	TEMED	0,04 % (w/v)
Sample buffer	95% Glycerol	42 %
	20% SDS	8 % (w/v)
	1,5m TRIS pH 6,8	279 mM
	2-mercaptoetanol	4 % (v/v)
	BTB	~0,1 mg/ml (w/v)
10x Running buffer	TRIS	250 mM
	Glycine	1,92 M
	0,1% SDS	1% (w/v)
	H_2O	
1x Transfer buffer	Trizima base	25 mM
	Glycine	192 mM
	Methanol	20 % (v/v)
	H_2O	80 % (v/v)
TBS-T	TRIS-HCl, pH 8,0	25 mM
	NaCl	125 mM
	Tween-20	0,1% (v/v)
Blocking buffer	TBS-T	97 % (v/v)
	Dried fat free milk	3 % (w/v)
Detection reagent A	100mM TRIS-HCL pH 8,5	100 mM
	Luminol	254 mM
	p-Coumaric acid (Enhancer)	15,5 mM
Detection reagent B	100mM TRIS-HCL pH 8,5	100mM
	30% H_2O_2 solution	1,8 mM
Incubation buffer	BSA	0,5 g
	PBS x1	100 ml

6.2.6 Solutions for lactate determination

Solution	Ingredients	Final concentration
Reagent A	163,64 mM Hydrazine	0,79 % (v/v)
	10,55 mM NAD^+	7,78 % (v/v)
	64,21 mM Glycine	6,42 % (v/v)
	H_2O	50,0 % (v/v)
	5M NaOH (adjusted to pH 9)	0,50 % (v/v)
	H_2O	35,0 % (v/v)
Reagent B	LDL (Lactate dehydrogenase)	13 enzyme units

6.2.7 Solutions used for the BrdU assay

Solution	Ingredients	Final concentration
BrdU labelling solution	BrdU labelling reagent (10mM) DMEM with 4,5g/L glucose, without L-Glutamine	As described in the manifacturers instructions
Anti-BrdU-POD stock solution	Anti-BrdU-POD milliQ H_2O (1,1ml)	
Anti-BrdU-POD working solution	Anti-BrdU-POD stock solution Antibody dilution solution	

6.2.8 Solutions used for the MTT assay

Solution	Ingredients	Final concentration
MTT stock solution	MTT 5mg PBS 1ml	As described in the manifacturers instructions
SDS-HCl solution	SDS 1g 0,01M HCl 10 ml	

6.2.9 Solutions for oxygraph measurements

Solution	Ingredients	Final concentration
Miro5	EGTA	0,190 g (0,5mM)
	$MgCl_2$ $6H_2O$	0,610 g (3 mM)
	K-lactobionate	120 ml of 0,5M stock (60 mM)
	Taurine	2,502 g (20 mM)
	KH_2PO_4	1,361 g (10 mM)
	HEPES	4,77 g (20mM)
	Sucrose	37,65 g (110 mM)
	BSA	1 g (1g/L)
	H_2O	To 1 litre

6.3 Molecular mass and size standards

Standard	Range	Supplier
Precision Plus Protein all blue standard (pre-stainded)	10-250 kDa	BioRad
MagicMark™ XP Western Protein Standard	20-220 kDa	Invitrogen

6.4 Antibodies used for protein determination

6.4.1 Primary antibodies used for flow cytometry

Antibody	Host	Working dilution	Supplier
Anti-phospho-Akt (Ser 473)	Rabbit	1:100	Cell signalling
Anti-phospho-Akt (Thr 308)	Rabbit	1:100	Cell signalling
Anti-Akt	Rabbit	1:100	Cell signalling
Anti-phospho-AMPK α (Thr 172)	Rabbit	1:50	Cell signalling
Anti-AMPK α	Rabbit	1:50	Cell signalling
Anti-phospho-AMPK β (Ser 108)	Rabbit	1:100	Cell signalling
Anti- AMPK β	Rabbit	1:50	Cell signalling
Anti-Acetyl-CoA Carboxylase	Rabbit	1:400	Cell signalling
Anti-phospho-Acetyl-CoA Carboxylase (Ser 79)	Rabbit	1:25	Cell signalling

6.4.2 EGFR vIII antibody used for flow cytometry and western blotting

Antibody	Host	Working dilution	Supplier
EGFR vIII	Mouse	1:200 (flow cytometry) 1:500 (western blotting)	Hrvoje Miletic

6.4.3 Secondary antibodies used for flow cytometry and western blotting

Antibody	Host	Working dilution	Supplier
Goat anti rabbit Alexa 647	Goat	1:1000	Invitrogen
Anti mouse horshradish peroxidise conjugated	Goat	1:5000	Biorad
Anti mouse APC	Goat	1:1000	Molecular probes

6.5 Fluorescent probes for Flow cytometry analysis

Fluorescent probe	Laser	Maximum excitation	Maximum emission	Detector	Supplier
NAO (acridine orange 10-nonyl bromide)	488	495nm	519nm	FL-1	Invitrogen
ROS (CM_2H_2DCFDA)	488	495nm	517nm	FL-1	Invitrogen
TMRM (Tetramethyl Rhodamine Methyl Ester)	488	549nm	577nm	FL-2	Invitrogen

6.6 Commercial kits

Kit	Supplier
Pierce® BCA protein assay kit	Thermo scientific
Vybrant® MTT Cell Proliferation Assay Kit	Molecular Probes®
Cell proliferation ELISA, BrdU (colorimetric)	Roche
AlamarBlue® Assay	BIOSOURCE™
Mito Tracker Deep Red 633	Invitrogen

6.7 Computer software

Software	Supplier
DigiRed	Microplate Instrumentation Control
FlowJo	FlowJo
BD CellQuest™	BD Biosciences
Quantity One	BioRad
KCjunior	Bio-Tek instruments
UltraView	Ultra View
ImageSuite	Microsoft
DatLab 4	Oroboros

6.8 Consumables

Consumable	Supplier
Cell culture flasks	Sarstedt, Nunc
96 welled adhesion test plates	Sarstedt, Nunc
Acrodisc® syringe filters	PALL corporations
1-25ml pipettes	Sarstedt
Syringes	Sabre
15/50 ml tubes	Sarstedt, Nunc, VWR
Microsentrifuge tubes	Brand
1-1000µl pipettes	Gilson, Finntip
Glass bottom microwell dishes	MatTec corporations

6.9 Technical equipment

Equipment	Supplier
BD FACSCalibur™ Flow Cytometer	BD biosciences
Centrifuge 5810R	Eppendorf
Fluor-S™ Multimager	BioRad
Haake W26/Haake DC10	Thermo
Hetomaster Shake	Comfort
Hotplate	Kervel
Lamin Air airflow cabinet	Nuaire
Vacusafe comfort	Vacusafe
HeraCell 150	Heracell
UVM340 ELISA reader	Asys
SpectraMAX, GeminiEM	Molecular Devices Corporation
CKX31SF light microscope	Olympus
Roller mixer	Stuart
Nikon Eclipse TS100 light microscope	Nikon
Transsonic T310 sonicator	Elma®
Mettler AT200	Mettler
CP2202S	Sartonius
691 PH-meter	Metrohm
OROBOROS Oxygraph-2k	Oroboros instruments
Drieblock DB	Techne
Locator 8 Plus	Thermolyne
PowerPac HC	BioRad
PowerPac 1000	BioRad
KL-2	Edmund Bukler
Rotamax 120	Heidolph
Mini-protean 3 electrophoresis cell for SDS-PAGE	BioRad
Mini-trans blot cell for western blot	BioRad
Magnet Strirrer	Cenco
MS2-Minishaker	IKA®
Minispinn	Eppendorf
Stir CB161	Stuart
Pipetboy Comfort	Integra Biosciences
Heracell 150	Heraeus
Bürker	Assistent
Zeiss LSB 510 Meta, confocal microscope	Carl Zeiss

7. Methods

7.1 Cell lines

7.1.1 U87 glioma cells

The U87 human glioblastoma cell line has an epithelial morphology and was a kind gift from Hrvoje Miletic. Glioblastoma multiforme (GBM) is the most common and aggressive brain tumor found in adults. GBM accounts for 52 percent of primary brain tumors and has a median patient survival time of 12 months from diagnosis [57]. EGFR is the most frequently altered gene within GBM, and is found to be overexpressed in 40-50 percent of the occasions. For nearly 50 percent of these cases the mutant EGFR variant III (EGFR vIII) is co-expressed, and the detection of EGFR vIII is often associated with poor patient prognosis [58, 59] Compared to the WT, EGFR vIII lack a region at the extracellular receptor domain making it unable to bind EGFR binding ligands. However, due to this structural manipulation, the receptor is constantly phosphorylated and able to activate downstream signaling pathways [60]. The mutated form is believed to act, at least in part, through different signaling cascades than the WT, and this may account for the increased malignancy for EGFR vIII expressing cells [61]. Since the EGFR vIII is only found in tumor cells it can prove to be an ideal target for anti cancer therapy.

7.1.2 3T3 fibroblast cells

3T3 cells are the standard fibroblast cell line and were originally obtained from mouse embryo tissue [62]. In the proliferation experiments the 3T3 cells were used as a reference.

7.2 Growth medium and cell maintenance

The adhesive glioma and fibroblast cells were grown in cell culture flasks and split every other day. The cells were kept in a tissue culture incubator in a humidified environment at $37^{o}C$ / 5% CO_2 in a Dulbecco's Modified Eagle's Medium (DMEM) added 10 % heat deactivated foetal bovine serum (FBS), 1 % L-glutamine and 1 % penicillin/Streptomycin (100x).

When maintaining the cells, the medium was removed and the cells were rinsed with PBS to remove dead cells and old medium. 4ml trypsin-EDTA (0,25%) and 3ml PBS was added to

detach the cells. The trypsin reaction was inactivated by adding an equivalent amount of culture medium. The cells were transferred to a 15 ml tube and centrifuged at 800rpm for 4 minutes (the supernatant was wasted and the cell pellet re-suspended) before approximately 3 million cells were added to the fresh medium in a cell culture flask.

7.3 Cryogenic preservation and storage

When preparing the cells for cryogenic preservation, cells were detached as previously described, counted and re-suspended in cryogenic medium to give a concentration of 1-3 x 10^6 cells/ml. 1 ml of the cell suspension were distributed into cryogenic vials. To avoid frigidity shock the cryogenic vials were placed in an isopropanol box lowering the temperature 1^{o}C per minute and stored in a -80ºC fridge for approximately 24 hours. For long time storage the cells were kept in liquid nitrogen at -170ºC.

Upon thawing, the preserved cells were gently heated to 37^{o}C. The cell suspension was resuspended in culture media and incubated in a 75 ml culture flask in a tissue culture incubator at 37^{o}C / 5% CO_2. The following day the culture medium was changed and the cells further maintained as previously described[63].

7.4 Oxygraph

The oxygraph is an excellent instrument for determination of oxygen consumption for various samples as cells, isolated mitochondria or tissue homogenates. Two samples can be run at the time as the instrument contains two separate chambers with oxygen sensors (electrodes). Before starting the experiment the cambers must be properly closed and all air bubbles removed to make sure that all oxygen consumed is delivered from the sample medium. Samples added to the chambers are kept at constant temperature and stirred to get an equal oxygen distribution. Being directly connected to the Oroboros DatLab4 computer software, the oxygen sensors can deliver real-time updates on the consumption rates and oxygen levels in the chambers. By sequential adding substrates and inhibitors of the ETC it is possible to analyze various aspects of mitochondrial function. The agents added during the experiment are listed in table 7.1.

Table 7.1 Agents added to the samples during oxygraph analysis

Chemical	Function
Oligomycin	Inhibitor of the ATP synthase. Used to determine the proton leakage through the inner mitochondrial membrane.
FCCP	FCCP is an uncoupler that allows proton flow through the mitochondrial matrix without ATP synthesis. Used to characterize the maximum respiratory capacity.
Rotenone	Inhibitor of NaDH-dehydrogenase at complex I by blocking the proteins electron transport properties. Used to determine complex I contribution in the ATP production.

7.5 Lactate assay

According to the Warburg legacy many cancer cells have an up-regulated glycolysis and an enhanced lactate production [15]. The lactate production indicates whether the malign cell uses glycolysis or mitochondrial respiration as their primary energy source. Therefore, lactate measurements are helpful when determining the nature of tumor cells.

Lactate secretion was determined by analyzing the cellular culture medium where cells had been grown for 48 hours. The collected medium was diluted with fresh DMEM culture medium without FBS to 6 different concentrations; 100%, 50%, 20%, 10%, 5% and 2.5% (used media: fresh media). 5 lactate standard solutions with the concentrations of 4mM, 3mM, 2mM, 1mM and 0.5mM were made and 20µl of all samples were transferred to a 96 welled test plate previously loaded with 170µl Reagent A solution. The hydrazine within this reagent destroys the pyruvate and allows complete oxidation of all lactate molecules. To ensure this, NAD^+ was provided in excess. The lactate concentration in the sample is proportional to the raise in absorbance as NAD^+ is reduced to NADH. The test plate was screened at 340nm using an EL_x808 Ultra Microplate ELISA Reader. 10µl lactate dehydrogenase (Reagent B = LDH) is added to the samples and the plate is incubated at room temperature for 60 minutes. The lactate dehydrogenase oxidizes the lactate back to pyruvate. Finally the 96 welled test plate is screened at the ELISA reader at 340 nm a second time. Calculations were carried out using the KCjunior computer software.

7.6 Cell proliferation assays

There are several proliferation assays that can be used in calculation and determination of cell growth properties. Here BrdU, alamarblue and MTT were compared to find the most suited assay for further analyses. For all the proliferation assays, measurements for U87 WT, U87 EGFR vIII and 3T3 cells were carried out. Exponentially growing cells were trypsinized, counted and diluted accordingly. For all assays the cells were plated with densities of 1000, 2000, 3000, 5000, 7000, 10000 and 15000 cells/well in a flat-bottomed 96-welled plate and stored for 24 hours at 37^{o}C / 5% CO_2 in a cell incubator. All cells were dissolved in 200µl culture media. Pure culture media was added to some wells to serve as a background. To include a negative control pure medium was treated in the same way as the cells. All absorbance measurements were carried out on a UVM340 ELISA reader and calculations were made using DigiRed computer software.

7.6.1 BrdU

Bromodeoxyuridine (BrdU) is a synthetic pyrimidine analogue that is incorporated into the DNA instead of thymidine in proliferating cells. BrdU specific antibodies detect the incorporated nucleoside, and by doing this measure replicated cells. The reaction product is quantified by colorimetric measuring the absorbance at the respective wavelength at an ELISA reader. The ability of BrdU to replace thymidine during DNA replication can cause genetic mutations, and it is therefore a potentially health hazard.

20µl 100µM BrdU labeling solution was added to each well before the plate was incubated for 4 hours at 37^{o}C / 5%. The culture media/labeling solution was removed and 200µl/well Fix Denat solution was added and cells incubated for 30 minutes at room temperature. The Fix Denat solution was tapped and 100µl/well anti-BrdU-POD working solution was added before the plate was incubated for 90 minutes at room temperature. The antibody solution was discarded and the wells rinsed 3 times using PBS. 100µl/well substrate solution was added and the samples were incubated at room temperature until color development is sufficient for photometric detection. Finally, the sample absorbance was measured at 370nm.
All steps in the assay were carried out according to the manufacturers' instructions.

7.6.2 Alamarblue

The assay contains an oxidation-reduction (REDOX) indicator that both changes color and fluoresces in response to cellular growth. The metabolic activity within the growing cell results in a chemical converting of reasazurin (the active ingredient in alamarblue) to resorufin. A continued growth of the cells maintains a reduced environment, while growth inhibition gains an oxidized environment. Growth related reduction causes the REDOX indicator to transform from the oxidized form (blue, non-fluorecent) to the reduced form (red, fluorescent). These cellular changes can be detected using an ELISA reader or a fluorescence spectrophotometer.

20µl/well alamarblue was added and the plate was further stored in the incubator. Colorimetric measures were accomplished after 2, 3, 4 and 24 hours at 570nm and 600nm respectively.

The percent of reduced AlamarBlue is determined by using equation 7.1:

$$\frac{C_{RED}\,\text{Test Well}}{C_{OX}\,\text{Negative Control Well}} = \frac{(\varepsilon_{OX})\lambda_2 A\lambda_1 - (\varepsilon_{OX})\lambda_1 A\lambda_2}{(\varepsilon_{RED})\lambda_1 A'\lambda_2 - (\varepsilon_{RED})\lambda_2 A'\lambda_1} \times 100$$

Equation 7.1. Used for the calculation of % reduced AlamarBlue from absorbance measurements.

Where,

C_{RED} = concentration of the reduced form AlamarBlue
C_{OX} = oxidized form of AlamarBlue
ε_{RED} = molar extinction coefficient of Alamar Blue reduced form
ε_{OX} = molar extinction coefficient of Alamar Blue oxidized form
A = absorbance of test wells
A' = absorbance of negative control wells
λ_1 = 570 nm
λ_2 = 600 nm

A fluorescent measurement was carried out 4 hours after alamarblue addition at 530nm excitation wavelength and at 590nm emission wavelength using a SpectraMAX, GeminiEM fluorescence spectrophotometer.

7.6.3 MTT – 3-(4,5-dimethylthiazol-2-yl)-2,5-diphenyltetrazolium bromide

The MTT (3-(4,5-dimethylthiazol-2-yl)-2,5-diphenyltetrazolium bromide) assay is one of the most versatile and popular assays used for cell growth rate determination. The assay includes the transformation of the water soluble MTT to purple, insoluble formazan crystals, a reaction carried out by viable cells.

Since the presence of phenol red in the final assay samples can seriously affect the results, a blank DMEM culture medium was used (DMEM without phenol red). After incubation the medium was removed and replaced with fresh culture medium before 20µl MTT stock solution was added. The stained cells were incubated for 4 hours at 37^{o}C / 5% CO_2 in a cell incubator, before 100µl/well SDS-HCl solution were added. The plate is thoroughly mixed using a pipette before incubated at 37^{o}C/5% CO_2 for another 18 hours. After incubation the samples are mixed before the absorbance is measured at 570nm on an UVM340 ELISA reader.

7.7 Flow cytometry

Flow cytometry is an analytic technology where particles or cells are suspended in a steam of fluid and transported through a laser beam. This technique can measure size, internal complexity, relative granularity and relative fluorescence intensity of particles/cells within the size range of 0.2 – 150 micrometers. Because flow cytometry can do multi parametric single cell analysis with a high throughput, it is a powerful tool within cell/particle characterization.

The flow cytometer has three main systems, fluidics, optics and electronics. The fluidic system is responsible for the transports of the particles to the laser beam for detection. In the optics lasers illuminate the particles and optical filters direct the scattered lights to the appropriate detectors. The electronic system detects the light signal and converts it into electric signals that analyzed by computer software.

When a sample is loaded into the flow cytometer it is surrounded by a sheath of fluid. The sample pressure is higher than the sheth fluid pressure, accelerating the particles and keeping them in the centre of the fluid stream. This process is known as hydrodynamic focusing and allows just a single cell/particle to be illuminated at the time, making it possible to observe heterogeneous differences in a cell population. Scattered light is measured using different detectors. Light passing through the sample is collected by the forward scatter (FSC) and is used for particle/cellular size determination. Side scattered light (SSC) is proportional to cell granularity or internal complexity. This refracted light is picked up in a 90^{o} angle to the laser beam. If the sample is stained with a fluorescent marker the emitted fluorescence is collected and guided to the appropriate detector depending on the wavelength of the emitted light (see

illustration in figure 7.1 for details).

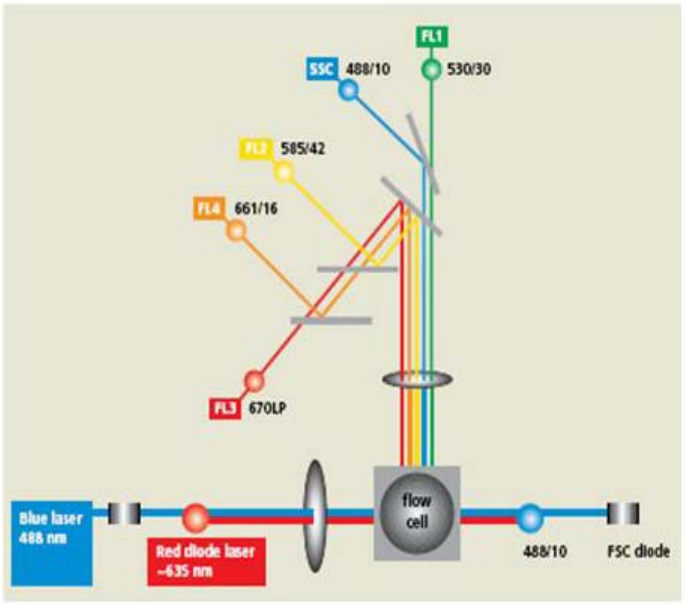

Detector	Wavelength (λ)	Colour
FSC	488nm	Blue
SSC	488nm	Blue
FL1	515 - 545nm	Green
FL2	564 - 606nm	Yellow
FL3	670nm -	Red
FL4	653 -669nm	Red

Figure 7.1. Optical bench diagram of the FACS Calibur flow cytometer. The figure is taken from the FACS Calibur instructions manual.

7.7.1 Cell characterization

The expression of EGFR vIII protein was determined by staining the cells with an EGFR vIII antibody. First, the cells were detached and counted as previously described and 4 samples were made for each cell line. $2x10^5$ cells in culture medium were transferred to micro-centrifuge tubes and added 1 ml PBS-0.2% BSA. The tubes were centrifuged at 700xG for 5 minutes, before aspirating the supernatant. The pellet are gently re-suspended in100µl EGFR vIII (1:200) in cold PBS-0.2% BSA, before incubated at room temperature for 30 minutes. The sample are rinsed using 1 ml cold PBS-0.2% BSA and centrifuged as described above. The supernatant is removed and the washing step repeated. The cells are re-suspended in 100µl goat-anti mouse APC secondary antibody (1:1000) in cold PBS-0.2% BSA and incubated for 30 minutes at room temperature in the dark. The samples are rinsed two more times and the samples re-suspended in 300µl cold PBS-0.2% BSA before FACS analysis. The antibody stained cells were detected in FL-4 (far red emission). Three different samples were measured for each cell line:

1. A control solution containing unstained cells.
2. A control solution only added secondary antibody
3. A solution stained with primary and secondary antibody. Here two parallels were made for each cell line.

7.7.2 Determination of mitochondrial properties by flow cytometry

Three fluorescent probes were used to measure mitochondrial characteristics for the wild type and mutated cell lines; Nonyl Acridine Orange (NAO), CM_2H_2DCFDA (ROS) and Tetramethyl Rhodamine Methyl Ester (TMRM). For all samples the cells were detached and the cell density adjusted to $1x10^6$ cells/ml in growth medium.

NAO is an appropriate marker of the inner mitochondrial membrane in whole cells. NAO binds to the negatively charged phospholipid cardiolipin which is only found in mitochondrial membranes. This can be used to measure mitochondrial content and observe mitochondrial biogenesis.
The NAO probes were added to give a final concentration of 200nM. In addition a NAO control solution containing 1mM FCCP was made and all samples were incubated for 15 minutes at 37°C / 5% CO_2. The NAO stained cells were cooled down on ice before centrifuged at 800rpm for 4 minutes. The supernatant was removed and the pellet re-suspended in 500µl cold PBS. The samples were transferred to FACS test tubes and the fluorescent emission was detected in FL-1 using the flow cytometer.

CM_2H_2DCFDA (ROS) is widely used to measure oxidative stress in cells. ROS is resistant to oxidation, but is de-acetylated by intracellular esterases when taken up by cells. This leads to the formation of the more hydrophilic, nonfluorescent dye dichlorofluorescin (DCFH). DCFH is then rapidly oxidized to form a two-electron oxidation product, the highly fluorescent DCF in a reaction with the oxidizing species (H_2O_2).
The ROS probe is made by diluting CM_2H_2DCFDA by DMSO to yield a final concentration of 5µM within the samples. A ROS control solution containing 100µM H_2O_2 was also made. The samples are incubated at 37°C for 30 minutes before fluorescence was detected in the FL-1 detector at the flow cytometer.

TMRM is a cationic, mitochondrial selective probe that can be used as a cytofluorometric method for analyzing the mitochondrial membrane potential ($\Delta\Psi m$). Being a key indicator of mitochondrial function the characterization of $\Delta\Psi m$ allows for an accurate determination of mitochondrial bioenergetics and cellular metabolism.
TMRM were added to the cell samples to give a final concentration of 200nM. In addition a control solution added 1mM FCCP was made for each cell line. The samples were incubated

for 30 minutes at 37°C before transferred to FACS test tubes. The emitted fluorescence was detected in the FL-2 detector using the flow cytometer.

10 000 cells/sample was analyzed using a BD FACS calibur™ flow cytometer and processed to the BD CellQuest computer software. Further analyses were done using FlowJo flow cytometry software.

Table 7.2 Probes and central information used for determination of mitochondrial properties

Probe	Concentration	Incubation time	Temperature	Control solution	Detector
NAO	200nM	15 min	37°C	2µl 1mM *FCCP*	FL-1
ROS	5µM	30 min	37°C	1µl 100µM H_2O_2	FL-1
TMRM	200nM	30 min	37°C	2µl 1mM *FCCP*	FL-2

7.7.3 Fixation of cells used for antibody staining

Cells were detached and collected as previous described, centrifuged for 4 minutes at 800 rpm before briefly re-suspended in 1ml 3.7% formaldehyde in PBS. The cells were fixated for 10 minutes before chilled on ice for 1 minute. The cell suspensions were pelleted by centrifugation, the fix was removed and the cells were permeabilized by adding ice-cold 100% methanol to a final concentration of 90 % methanol. After 30 minutes incubation on ice the cells were ready for antibody staining.

Upon antibody staining $0.5 \cdot 10^6$ cells were transferred into each assay tube. 2 ml incubation buffer was added to the tubes and rinsed by centrifugation. The rinsing procedure was repeated before the cells were re-suspended in 100µl incubation buffer and blocked for 10 minutes at room temperature. The primary antibody was added at appropriate dilution to the assay tubes and incubated at 60 minutes at room temperature. (Antibody dilutions can be seen in section 6.4 in Materials.) The cells were rinsed by centrifugation as previously described. Finally the secondary antibody diluted in incubation buffer was added to each tube and cells are incubated for 30 minutes at room temperature. Cells were rinsed and re-suspended in 0.5 ml PBS before analyzed at the FACS Calibur flow cytometer.

7.8 Cell lysis, protein determination, SDS-PAGE & Western Blotting

7.8.1 Cell lysis and protein determination

Approximately $1x10^7$ cells were transferred to a 15 ml test tube and centrifuged at 800 rpm for 4 minutes. The medium was removed and the pellet re-suspended in PBS before the centrifugation were repeated. Afterwards the cells were put on ice and dissolved in 500µl RIPA lysating buffer. The samples were incubated on ice for 2 minutes before centrifuged at 4000rpm for 5 minutes. The cell lysate was transferred to autoclaved eppendorf tubes and the protein concentration determined by using a Pierce© BCA Protein Assay Kit and spectro-photometric analysis (562nm at the UVM340 ELISA reader).

The protein concentration of the protein samples were determined by a set of protein standards. These standards were made by BSA (bovine serum albumine) diluted in RIPA buffer to yield final BSA concentrations of 2000, 1500, 1000, 750, 500, 250, 125, 25 and 0 µg/ml. The lysate of the two cell lines were diluted by RIPA buffer to give final lysate concentrations of 100%, 50%, 20%, 10% and 5%. 25µl of the standard solutions and protein samples were translocated to a 96 welled plate.
200µl working reactant solution from the protein assay kit was added to each well and the plate was mixed thoroughly on a plate shaker for 30 seconds, before covered and incubated for 30 minutes at 37°C. The plate was cooled to room temperature before the absorbance was measured at 562 nm using the UVM340 ELISA reader.
The absorbance values found were used to draw a standard curve for the BSA protein standard. This data was used together with the protein sample absorbance values to determine the protein content within the WT and the EGFR vIII cell line.

7.8.2 Sodium dodecyl sulphate polyacrylamide gel electrophoresis (SDS-PAGE)

SDS-PAGE is one of the major techniques in protein analysis, and here proteins are electrophoresed into a gel and separated based upon size and charge as they migrate through the gel. Smaller proteins characteristically migrate through the gel faster than larger protein. The sample buffer is made up by TRIS, SDS, BTB and mercaptoetanol. The Sample buffer was added to the cell lysate samples by a factor of 1:4, before they were heated for 5 minutes at 95°C. To ensure an appropriate mix the samples were vortexed and sonicated for a few minutes. Finally, the solutions were centrifuged for 5 minutes to avoid that impurities within the samples were added to the gel.

The polyacrylamide gels used to separate the sample proteins was made and run using a BioRad "mini-gel" system. The gels consisted of a 4% acrylamid stacking gel and a 10% acrylamid separation gel and were 1 mm tick. The two components of the gel have different tasks; the upper stacking gel compresses the added samples into thin layers, while the lower separation gel function to separate the proteins according to size. The chosen acrylamid content depends on the size of the protein to be identified in the sample. The smaller the known weight, the higher acrylamide percentage should be used. As references for the added protein samples a "BioRad Precision Plus Protein All Blue Standard" (protein standard) and a "Invitrogen MagicMark XP Western Protein Standard" (western blot standard) were added to each gel. The gel electrophoresis was run at room temperature at 200V in 1x running buffer. The electrophoresis was carried out until the lower molecular weight proteins had diffused through the gel. This was observed using the added protein standard. The approximate running time was 90 minutes.

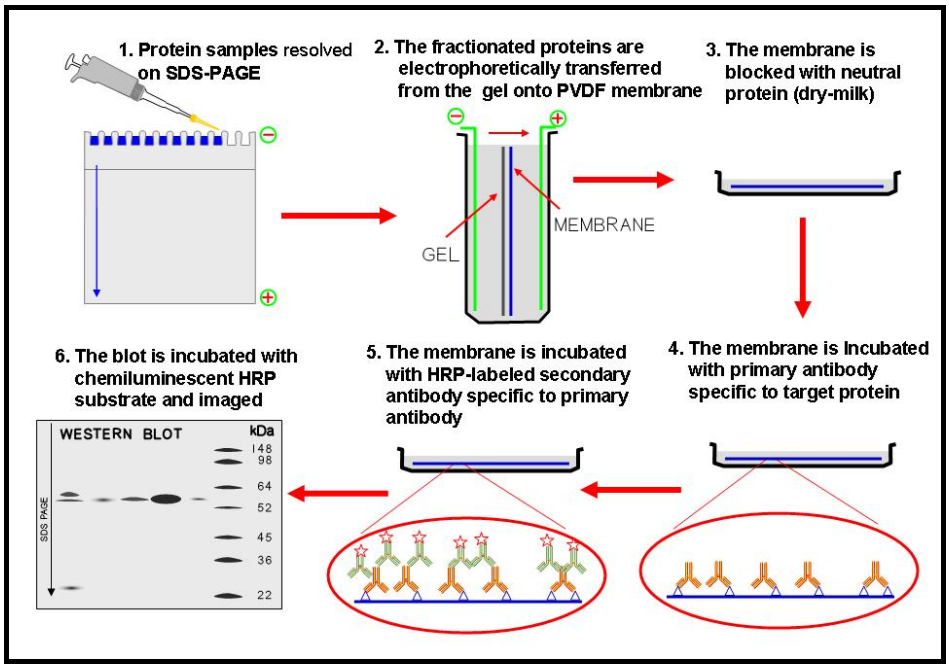

Figure 7.1 The procedure for SDS-PAGE and Western blotting. The presented illustration is taken from ScienceSlides, PowerPoint.

7.8.3 Western blotting

When identifying the proteins, specific antibodies are used to detect their antigen. Because of the specificity within antibody-antigen interaction, a single protein may be identified in a welter of protein mixture. Usually western blotting is used to positive identify a protein within a complex sample.

Following SDS-PAGE the gel is translocated into transfer buffer where it is kept for 10 minutes. By using a BioRad tank transfer system the proteins are translocated onto a nitrocellulose membrane. The procedure was run at 4^{o}C and at a constant voltage (19V, 2 ampere) for 12 hours. Afterwards, the membrane was transferred to a TBS-T–MLK blocking solution at room temperature for 2 hours to avoid unspecific binding of antibodies. When the blocking was completed the primary antibody diluted in TBS-T–MLK was added and the membrane was incubated at 4^{o}C overnight. The membrane was rinsed for 10 minutes using TBS-T–MLK and for 3 x 10 minutes in TBS-T before addition of the secondary antibody (also diluted in TBS-T–MLK). At last the membrane was washed 3 x 10 minutes in TBS-T before stored in milliQ.
When detecting the protein bound antibodies, the membrane was removed from the milliQ and added detection reagent A and B, before incubated at room temperature for 1 minute. A Bio-Rad Fluor-S multiimager was used for imaging and QuantityOne computer software for analyzing.

A Ponceau–S red staining solution was added to the membranes to verify a successfully transfer of proteins to the membrane. Here the blots were stained in the Ponceau-S red solution for 30 seconds before they were rinsed using milliQ. Finally scanned images of the blots were taken.

7.8 Immunostaining for imaging

Cells were trypsinated and collected as previously described. Approximately 50.000 cells (measured pre volume) were translocated to a culture dish with a fitted cover slip, 2 ml culture media were added and the cells were grown over night at 37^{o}C / 5% CO_2 in a cell incubator. Next morning 2µl 100µM mito tracker deep red (MRDR) (final concentration of 0.1 µM) were added and the cells were incubated at 37^{o}C/ 5% CO_2 for 30 minutes. The cells were gently rinsed using previously heated culture medium lacking phenol red supplied with 10% FBS. Afterwards the cells were added 1ml culture medium lacking phenol red and imaged using a Zeiss LSM 510 Meta confocal microscope connected to Ultra View computer software. The images were processed using ImageSuite software.

8. Results

8.1 Characterization of cell models

The two cell lines used in these experiments were U87 WT and U87 EGFR vIII isolated from human glioblastoma. To determine that the EGFR vIII expression indeed was elevated in the modified U87 glioma cell line (U87 EGFR vIII), we measured the EGFR vIII expression using flow cytometry and western blotting.

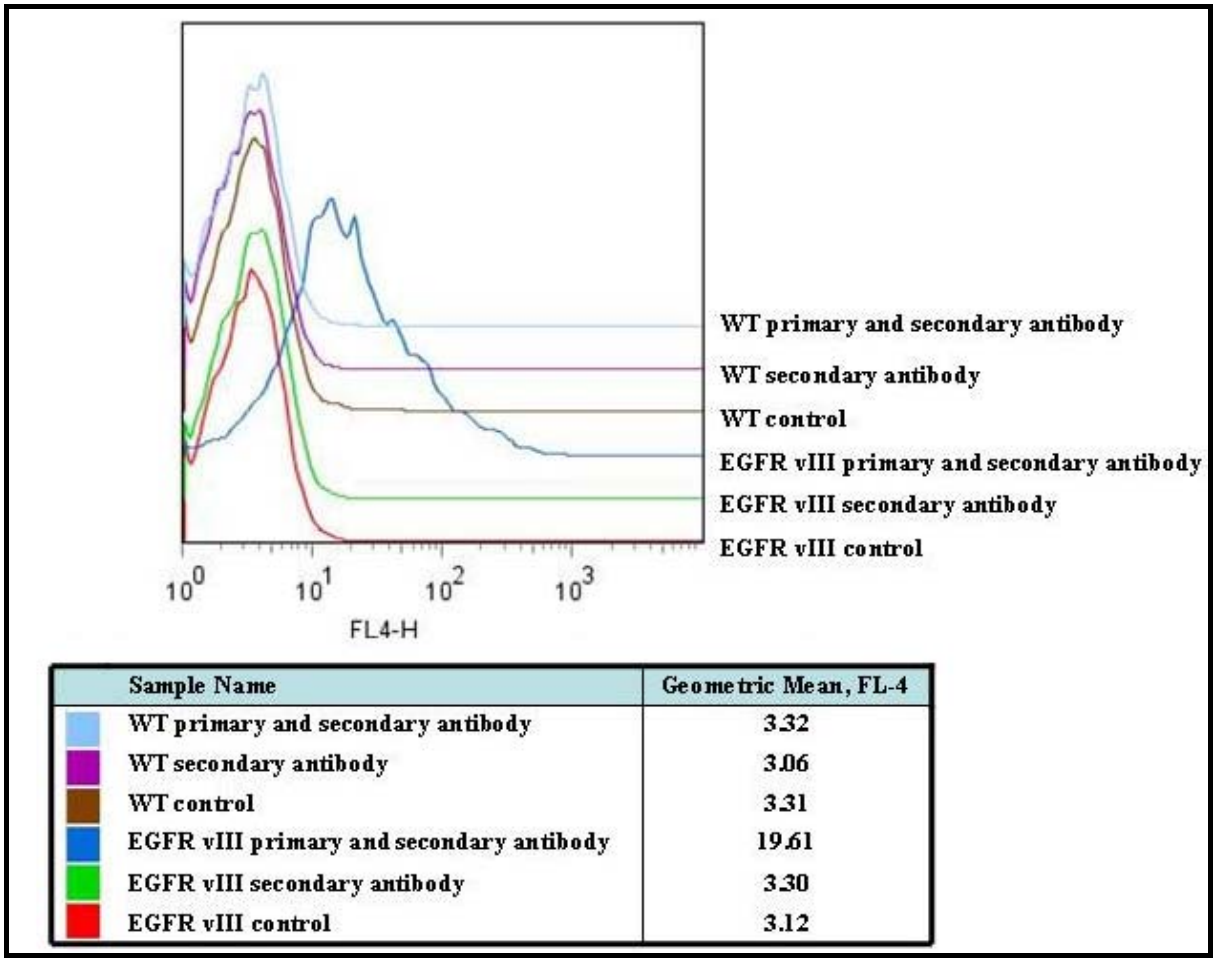

Sample Name	Geometric Mean, FL-4
WT primary and secondary antibody	3.32
WT secondary antibody	3.06
WT control	3.31
EGFR vIII primary and secondary antibody	19.61
EGFR vIII secondary antibody	3.30
EGFR vIII control	3.12

Figure 8.1. Results of EGFR antibody staining by flow cytometry. The dilution of the EGFR vIII antibody was 1:200 and the dilution of the anti-mouse APC secondary antibody was 1:5000. The curves shown are for unstained control cells, cells stained with a secondary antibody only, and cells stained with a primary and a secondary antibody for EGFR vIII and WT cell lines.

The curves presented in figure 8.1 show the content of stained EGFR vIII protein within the different samples. The curve for the EGFR vIII cells stained with both primary and secondary antibody is displaced (dark blue) compared to the remaining samples, showing a raised EGFR expression for the manipulated cells.

The results determined by the Western blots confirm the observations found by flow cytometry. As seen in figure 8.2 the four wells containing proteins from the mutated cells (well 4, 5, 8 and 9) show a defined expression pattern for EGFR vIII. We can also see that the wells containing 60µg proteins/well (well 8 and 9) have a stronger signal compared to wells containing 40µg proteins/well (well 4 and 5).

To confirm equal protein loading for each sample it is common to use the ubiquitously expressed actin as a marker. Here we used the dazo sodium salt Ponceau-S to check the protein levels. This was done since the size of EGFR vIII was 140 kDa and the SDS-PAGE was run such that the actin bands were no longer present on the gel for detection.

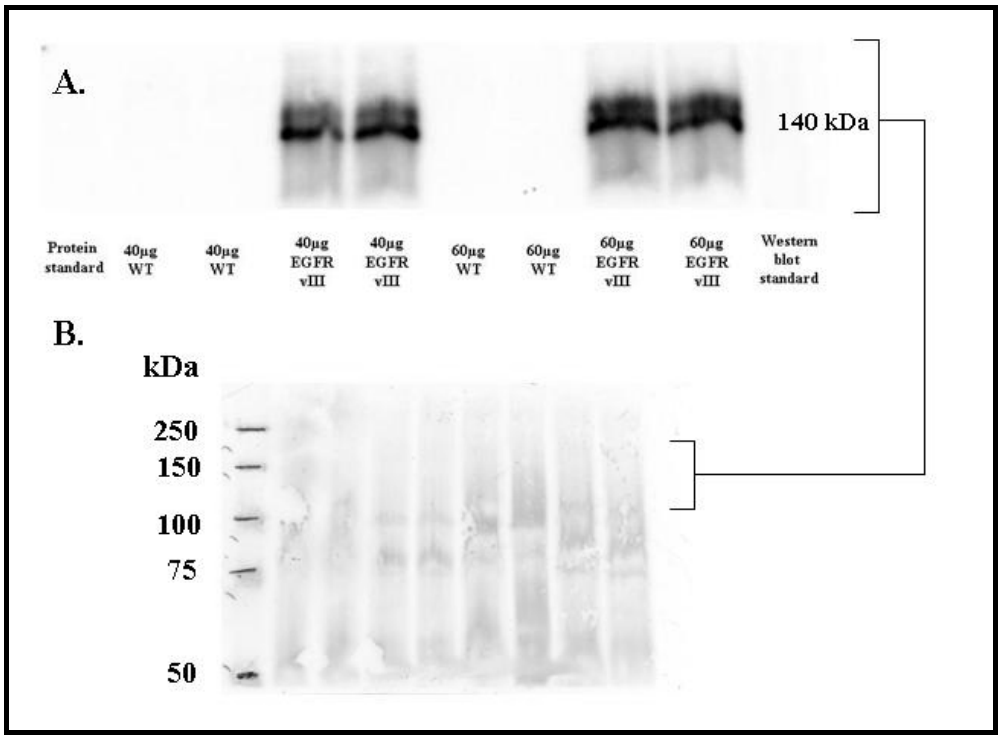

Figure 8.2. Expression of EGFR vIII in WT versus mutated cells.
U87 WT and EGFR vIII cell were lysed and protein content determined. For further calculations see appendix page 1. Afterwards the whole cell lysates were separated on SDS-PAGE, followed by immunoblotting using an EGFR vIII antibody. Two parallels were carried out, both presenting the same trend. **(A)** The western blot image was taken using a Bio-Rad Fluor-S multiimager. Two different protein concentrations were loaded to the gel together with a BioRad Precision Plus protein all blue protein standard and an Invitrogen MagicMark XP western protein standard. The blot was stained with EGFR vIII antibody diluted to a final concentration of 1:500, blocked with TBS-T/Mlk before stained with the anti-mouse horshradish peroxidase conjugated secondary antibody diluted 1:5000.
(B) Scanned image of the blot after Ponceau–S red staining.

Both the results found by flow cytometry and western blotting show an increased expression of EGFR vIII protein in the EGFR manipulated cells (EGFR vIII) compared to the WT. The Ponceau-S staining confirmed that the difference seen in EGFR vIII expression was not due to unequal protein loading in the western blot experiment.

Mitochondrial morphology in WT versus U87 EGFR vIII glioma cells

Confocal images were taken to see whether increased expression had an impact on mitochondrial morphology. These images were studied for obvious visual differences between the two cell lines (Figure 8.3 and 8.4). In both cell lines the mitochondria were distributed mainly around the nucleus, furthermore the mitochondrial network was filamentous rather than fragmented. No obvious differences between the WT and the EGFR vIII overexpressing cells were found.

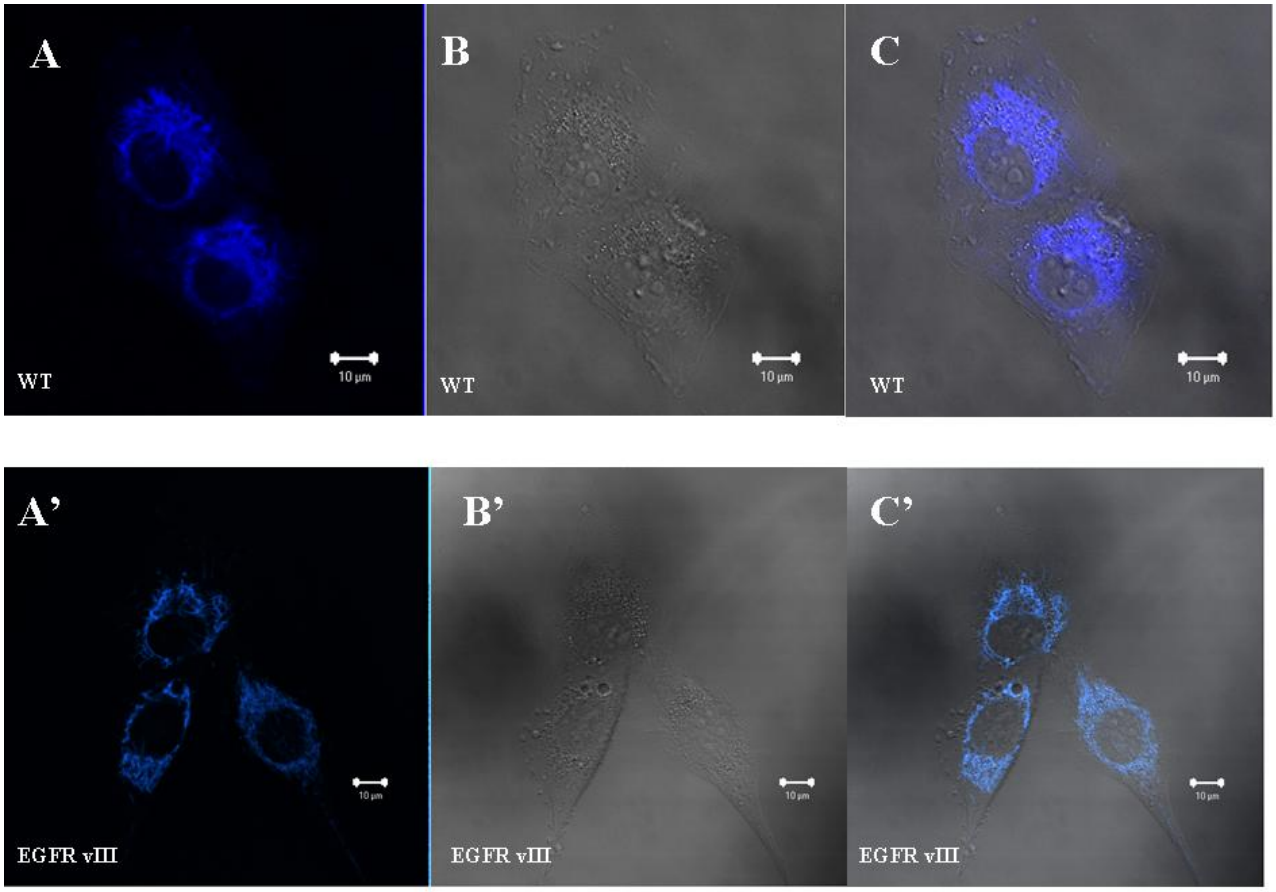

Figure 8.3. Images of U87 WT and EGFR vIII glioma cells. 50.000 cells were plated on a culture dish with a fitted cover slip and cultured over night at 37°C/5% CO_2 in a cell incubator. Following morning the cells were stained with a final concentration of 100nM Mitotracker DEEP red (MTDR) for 30 minutes at normal culture conditions before the medium was exchanged for DMEM medium without phenol red. Images were acquired using a Zeiss LSM 510 Meta confocal microscope using a 63x immersion objective. 5 images were taken and examined for each cell line. The presented image is representative for the findings. **(A/A')** MTDR image **(B/B')** Differential interference contrast (DIC) image **(C/C')** Overlay.

8.2 Metabolic profiling

Oxygraph data

Oxygraph measurements were carried out to look for possible differences in the respiratory capacity between the two cell types. These results are presented in figure 8.4. From these data a higher routine activity and maximum respiratory capacity was observed for the WT compared to EGFR vIII cells. These measurements also showed that the WT cell line used a smaller fraction of its maximum respiratory capacity under normal conditions.

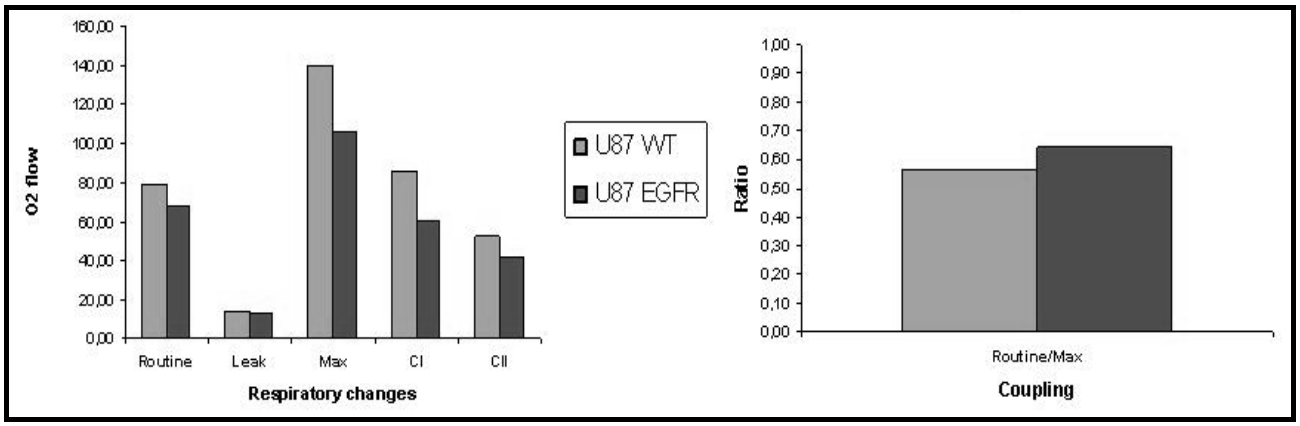

Figure 8.4. Metabolic data obtained from oxygraph measurements. Here Routine indicates the cellular respiratory capacity under normal conditions when glutamate and malic acid are present. Leak is O_2 flow gained from protons entering the mitochondria through alternate channels than the ATP driven complex V. This is measured by adding the complex V inhibitor oligomycine. Max respiratory capacity is determined by adding the uncoupler FCCP. The contribution from complex II is measured by adding the complex I inhibitor rotenone. Maximum complex I capacity is calculated by subtracting the Complex II O_2 flow from maximum respiratory capacity. The second diagram show how much of the maximum capacity the cells use under normal conditions by dividing the routine capacity on maximum respiratory capacity. These results were acquired using an Oroboros Oxygraph-2k.

Lactate secretion

Lactate is an indicator product of anaerobic glycolysis. We measured the amount of lactate secreted by the two different cell models under normal conditions. According to figure 8.5 EGFR vIII cells show a 15-35 % raise in lactate production compared to the WT cell line which may indicate an increased glycolytic activity within EGFR vIII cells. Further results and calculations can be seen in the appendix page 2

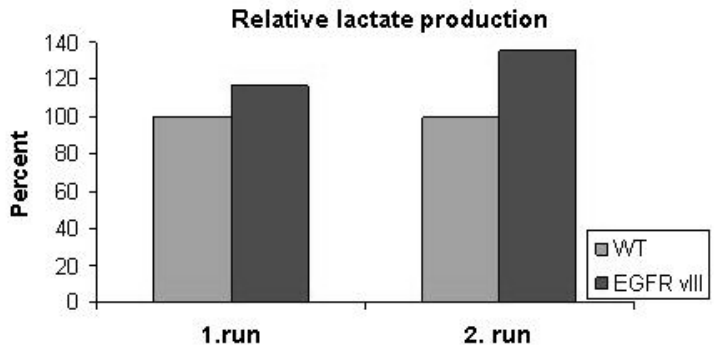

Figure 8.5. Lactate production in U87 WT and U87 EGFR vIII cells. The cells were counted and the lactate secretion was determined using culture medium in which the cells had been grown in for 48 hours. A number of lactate standards and different dilutions of the culture media were plated in a 96 welled plate before the absorbance were measured using an EL_x808 Ultra Microplate Reader. The lactate assays was carried out using medium from two distinct dates, hence 1.run and 2.run. The results are shown as relative percent values of the WT values for each run.

8.3 Proliferation and the metabolic interactions. Evaluation of the proliferation assays

Cell proliferation assays

The observed variations in lactate secretion and respiration for WT and manipulated cells suggested that EGFR may regulate energy metabolism. To see if this also affects cell growth we investigated if there was a correlation between cell proliferation and EGFR vIII expression. Three effective and well known assays were used to determine the proliferation properties of the cell lines; MTT, BrdU and AlamarBlue. These assays employ different analytical principles (see matherials and methods) which may give additional information about the physiological status of the cell population. For these studies 3T3 fibroblast cells were used as a reference cell line. In addition to compare the proliferation patterns these data were used to determine the most suited cell density for further analyses.

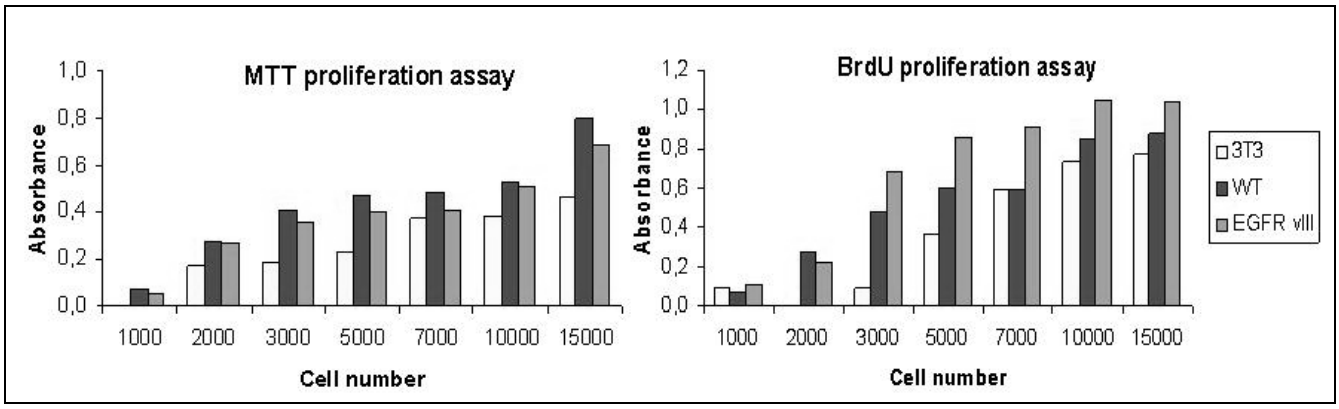

Figure 8.6. Results of the MTT and BrdU proliferation assay. The cells were plated with different cell densities (1000 – 15000 cells/well) in a flat-bottomed 96-welled plate and kept for 24 hours at 37°C/5% CO_2 in a cell incubator. The proliferation assays were accomplished according to the manufactory instructions and the absorbance was determined using an Asys UVM340 ELISA reader (MTT was measured at 570nm, while BrdU was measured at 370nm with a reference wavelength at 492nm). Four parallels of each sample were plated and the average of these parallels is shown in the diagram.

Using the fact that proliferation correlates with absorbance in these assays, the data above show a cell density dependent increase in proliferation for all the three cell lines. Data from the MTT assay show a slightly higher proliferation rate for the WT cells, while EGFR vIII had a higher rate using the BrdU assay. For both assays 3T3 cells had lower proliferation rates than the U87 cells.

Alamarblue has dual properties and can be measured by either fluorescence or absorbance. Here, both characteristics were tested and the proliferation trends compared. The absorbance was measured for the three cell lines after 2, 3, 4 and 24 hours, by reading at the two different wave lengths 570 nm and 600 nm.

The fluorescent properties were determined 4 hours after AlamarBlue addition. As seen in figure 8.8A the U87 glioma cells (WT and EGFR vIII) seem to have higher activity compared to the fibroblast cell line. As for the absorbance measurements the fluorescence raises with increased cell number.

The absorption data found are shown in Figure 8.8 B, C, and D. All three cell lines displayed a cell number and time dependent increase in the signal following 2-4 h of incubation. However, after 24 h the maximum Alamarblue signal was reached with the higher cell numbers, as seen by the cell density dependent flattening of the curve.

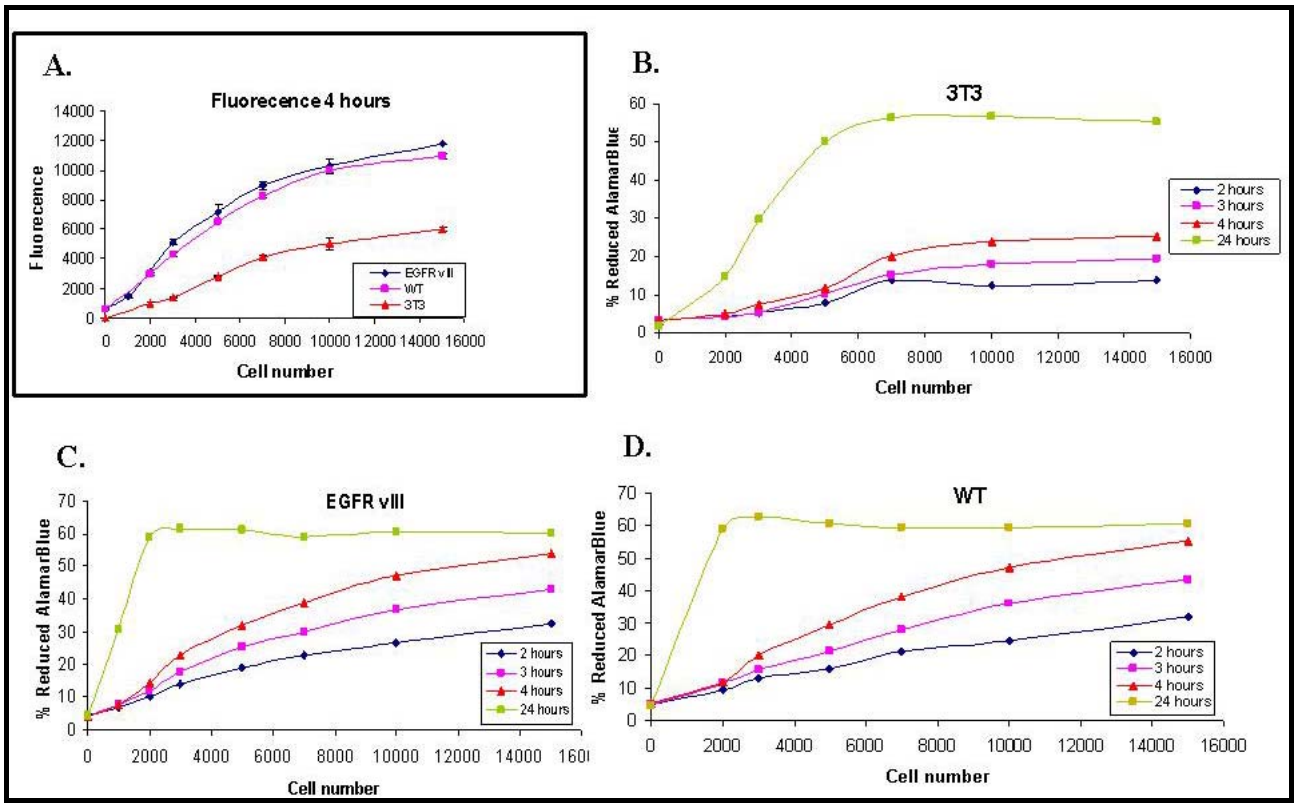

Figure 8.7. Results of the AlamarBlue assay. The cells were plated with different cell densities (1000 – 15000 cells/well) in a flat-bottomed 96-welled plate and incubated for 24 hours at 37°C/5% CO_2 in a cell incubator. **(A)** fluorescent analysis at 4 hours after AlamarBlue addition. Absorbance measurements were carried out at 2 (blue), 3 (pink), 4 (red) and 24 (green) hours after AlamarBlue addition respectively. % reduced AlamarBlue were calculated using equation 8.1. **(B)** % reduced AlamarBlue of 3T3 cells, **(C)** % reduced AlamarBlue of U87 EGFR vIII cells and **(D)** % reduced AlamarBlue of U87 WT cells. Four parallels of each sample were plated and the average of these parallels is shown in the curves.

To compare the three different assays the proliferation data were put into the same diagram. Here the values are relative to the maximum value at 15000 cells for its respective proliferation assay. According to the curves in figure 8.8, the proliferation assays show the same trend when using MTT, BrdU or AlamarBlue.

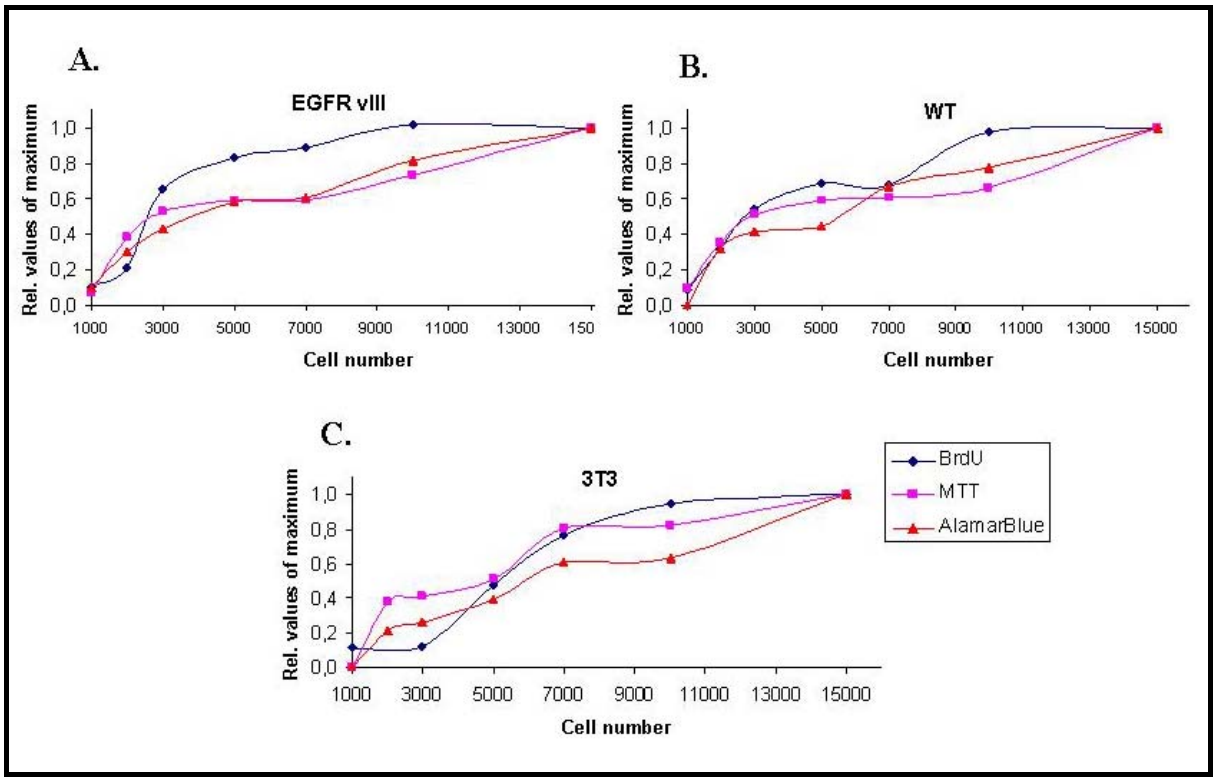

Figure 8.8. Relative values of MTT, BrdU and AlamarBlue proliferation assays. For each cell line the data from the three assays were put into the same diagram. The AlamarBlue absorbances are from the 4 hour experiment. **(A)** Relative proliferation values for EGFR vIII, **(B)** WT and **(C)** 3T3 cell line respectively.

Once the proliferation characteristics had been found, these data were used to determine the most suitable cell number for further trials. This concentration has to be in an area where the proliferation curves are linear. These conditions are favourable because they indicate a constant proliferation with a low fraction of apoptosis and abundant levels of nutrients are present. According to these data such conditions exist in the range between 3000 and 7000 cells/well. Consequently, we chose to use 4000 cells/well for further experiments.

8.4 Effects of metabolic manipulation on cell proliferation

Rotenone treatment

Having determined the proliferation properties of the cells, we then asked whether the WT and manipulated cell line had differences in the metabolic regulation.
Rotenone is an inhibitor of complex I in the Electron transport chain (ETC). The rotenone sensitivity is an indicator of how the cells depend on respiration for energy production. Rotenone treatment may also show the cellular ability to switch to an alternate energy pathway when the mitochondrial respiration is inhibited.

These trials were used to find the rotenone concentration in which 50% of the proliferation was inhibited (IC_{50}).To determine the IC_{50} value we used the MTT and BrdU proliferation assays.

Cells were treated with rotenone concentrations ranging from 0.05-10µM. The 10µM concentration was used to fully "shut down" the contribution from complex I in the ETC. Despite similar experimental conditions, major variations in mitochondrial blockage response were observed for the three accomplished experiments. A metabolic interaction between MTT and rotenone was suspected, making MTT an inappropriate assay for proliferation measurements on rotenone treated cells. One of the experiments is shown in figure 8.9.

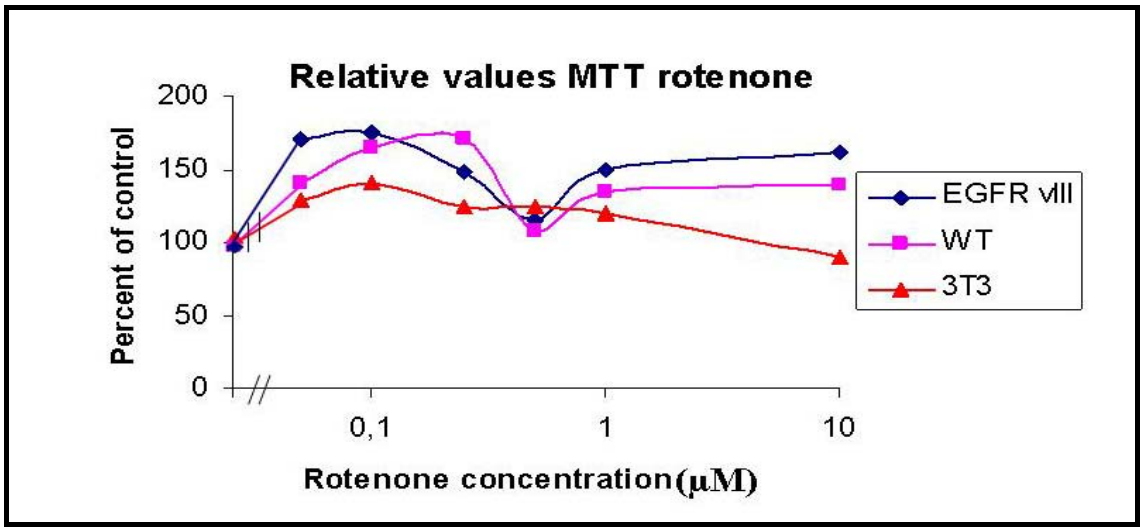

Figure 8.9. Curves of rotenone treated cells using MTT proliferation assay. 4000 cell/well were plated in a flat-bottomed 96-welled plate and cultured for 24 hours at 37°C/5% CO_2 in a cell incubator. The cells were then treated with different rotenone concentrations of 0.05µM, 0.1µM, 0.25µM, 0.5µM, 1µM and 10µM and stored for 20 hours at 37°C/5% CO_2. Four parallels of each sample were plated and the average of these parallels is shown in the diagram.

Since MTT failed to function as appropriate assay for rotenone treated cells, BrdU was the only proliferation assay used for further rotenone analyses. The same rotenone concentrations as for MTT were used to inhibit the mitochondrial respiration.

These trials were carried out 5 times, but due to experimental problems, the mean of 3 successful experiments are shown in figure 8.10. From these data we see a significant difference in rotenone sensitivity. The EGFR vIII cells are more affected by respiratory blockage and have an IC_{50} value at approximately 0.1µM rotenone. According to these findings WT and 3T3 cells are more resistant to the rotenone treatment with an IC_{50} value at approximately 1µM.

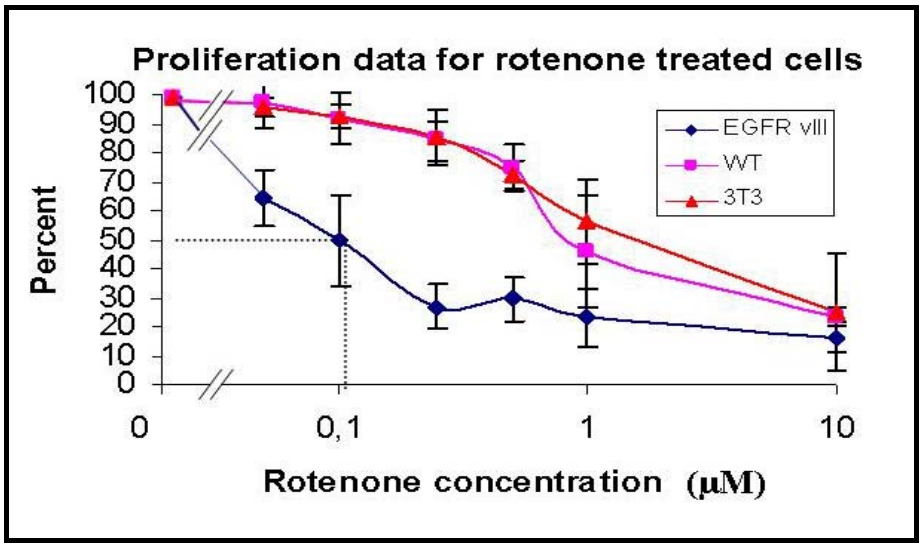

Figure 8.10. Determination of EGFR vIII rotenone IC_{50} value. 4000 cell/well were plated in a flat-bottomed 96-welled plate and incubated for 24 hours at 37°C/5% CO_2 in a cell incubator. The cells were then treated with different rotenone concentrations of 0.05µM, 0.1µM, 0.25µM, 0.5µM, 1µM and 10µM and stored for 20 hours at 37°C/5% CO_2 in a cell incubator. Four parallels of each sample were plated and the average of these parallels is shown in the diagram. All values are shown as relative percent values of the untreated control cells.

2DG treatment

Since rotenone treatment indicated differences in the mitochondrial respiration, we wanted to look at proliferation response when blocking the glycolytic energy pathway. Here the U87 cells were treated with the hexokinase inhibitor 2-deoxy glucose (2DG), using concentrations within the range 0.15 - 10µM.

Three experiments were accomplished and are shown in figure 8.12. Here, two experiments were carried out at high 2DG concentrations and one representative curve is presented. Here the proliferation rate increased before a sudden drop was seen. The instant fall made it difficult to determine the 2DG IC_{50} value and therefore an experiment at lower 2DG concentrations were carried out. Using data from the third experiment, the IC_{50} value of the

EGFR vIII cells was found to be approximately 1 µM 2DG. From these trials the WT and the EGFR vIII cells show a similar response to 2DG inhibition of the glycolysis.

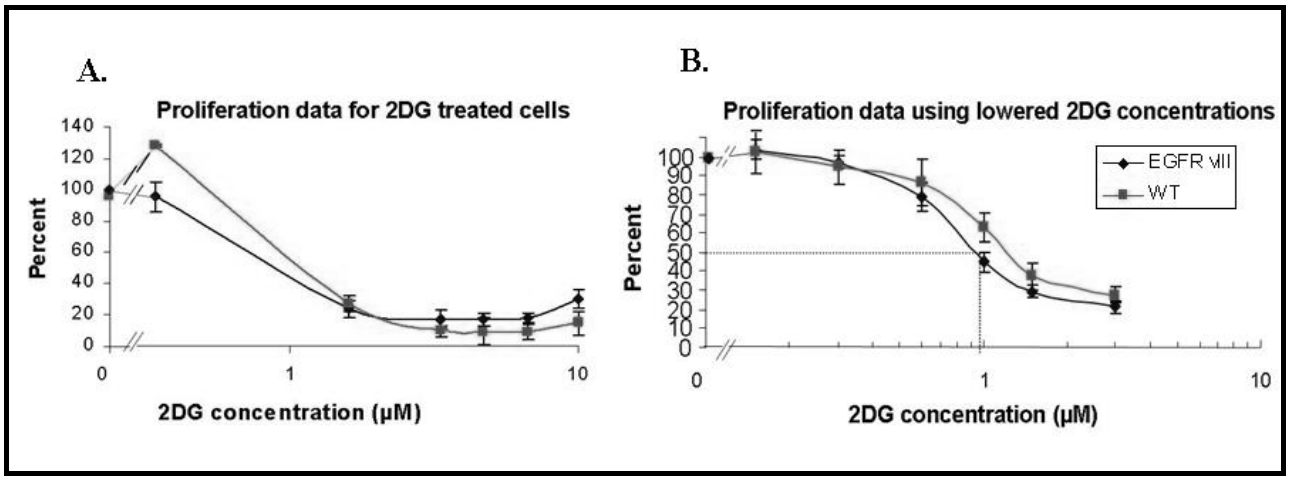

Figure 8.11. Determination of EGFR vIII 2DG IC_{50} value. 4.000 cell/well were plated in a flat-bottomed 96-welled plate and kept for 24 hours at 37°C/5% CO_2 in a cell incubator. The cells were then treated with different 2DG concentrations (0.34µM, 1.6µM, 3.34µM, 4.66µM, 6.67µM and 10µM presented in A., 0.15µM, 0.3µM, 0.6µM, 1.0µM, 1.5µM and 3µM in experiment B.) and stored for 20 hours at 37°C/5% CO_2 in a cell incubator. Six parallels of each sample were plated and the average of these parallels is shown in the diagram.

8.5. Effect of rotenone and 2DG treatment on lactate secretion

In the previously experiments the EGFR vIII IC_{50} concentrations for rotenone and 2DG were determined. Further, we wanted to see whether these treatments could affect the lactate secretion in a different manner between the two cell lines cells. The lactate concentration were determined in WT and EGFR vIII control cells and in cells treated with 0.5µM 2DG, 1µM 2DG, 500nM rotenone and 0.1µM rotenone.

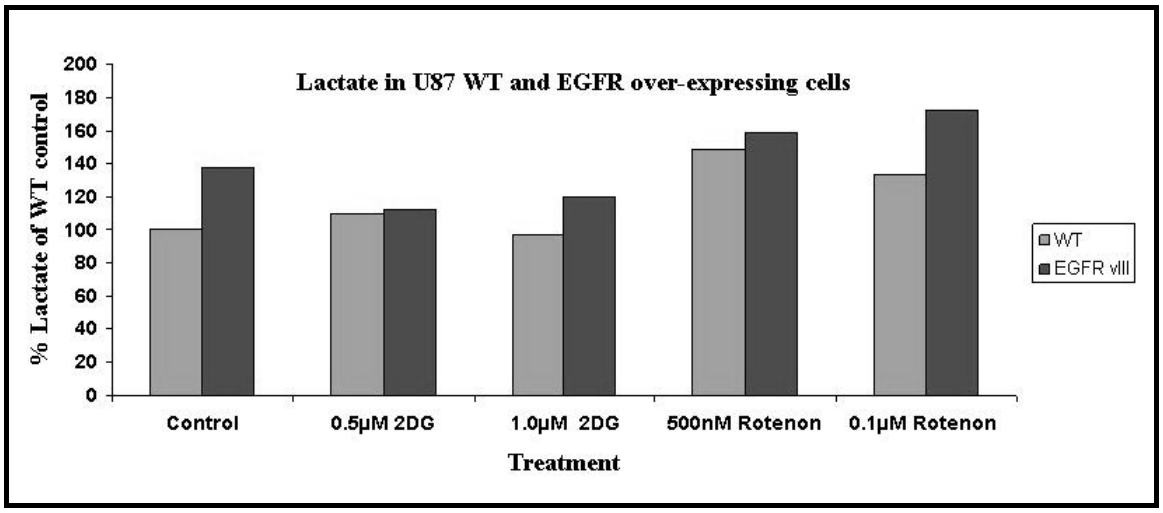

Figure 8.12 Lactate measurement of 2DG and rotenone treated cells. The cells were grown in a culture flask for 24 hours before treated for another 24 hour with rotenone or 2DG. During this time the flasks were kept at 37°C/5% CO_2 in a cell incubator. Further, culture medium was collected for lactate analysis. A number of lactate standards and different dilutions of the culture media were plated in a 96 welled plate before the absorbance were measured using an EL_x808 Ultra Microplate Reader. The results are shown as relative percent values of the WT control.

Upon glycolytic inhibition by 2DG, the lactate secretions by WT cells are approximately the same as control, while the mutated cell line shows a minor decrease. When blocking the respiration energy supply by rotenone, the lactate production is raised for both cell lines. This experiment show an elevated EGFR vIII secretion of lactate compared to WT cells when treated with rotenone. Further results and calculations can be seen in the appendix page 4

8.6 Effects of metabolic inhibitors on proliferation related signalling

Determination of protein signalling using antibodies

Based on the above findings it was interesting to investigate factors that may connect regulation of cell proliferation with metabolism. We chose to study the expression patterns of common signalling pathways found in cancer cells. Here represented by Akt, AMPK α, AMPK β and ACC proteins, which are all involved in regulating cellular metabolism and energy production.

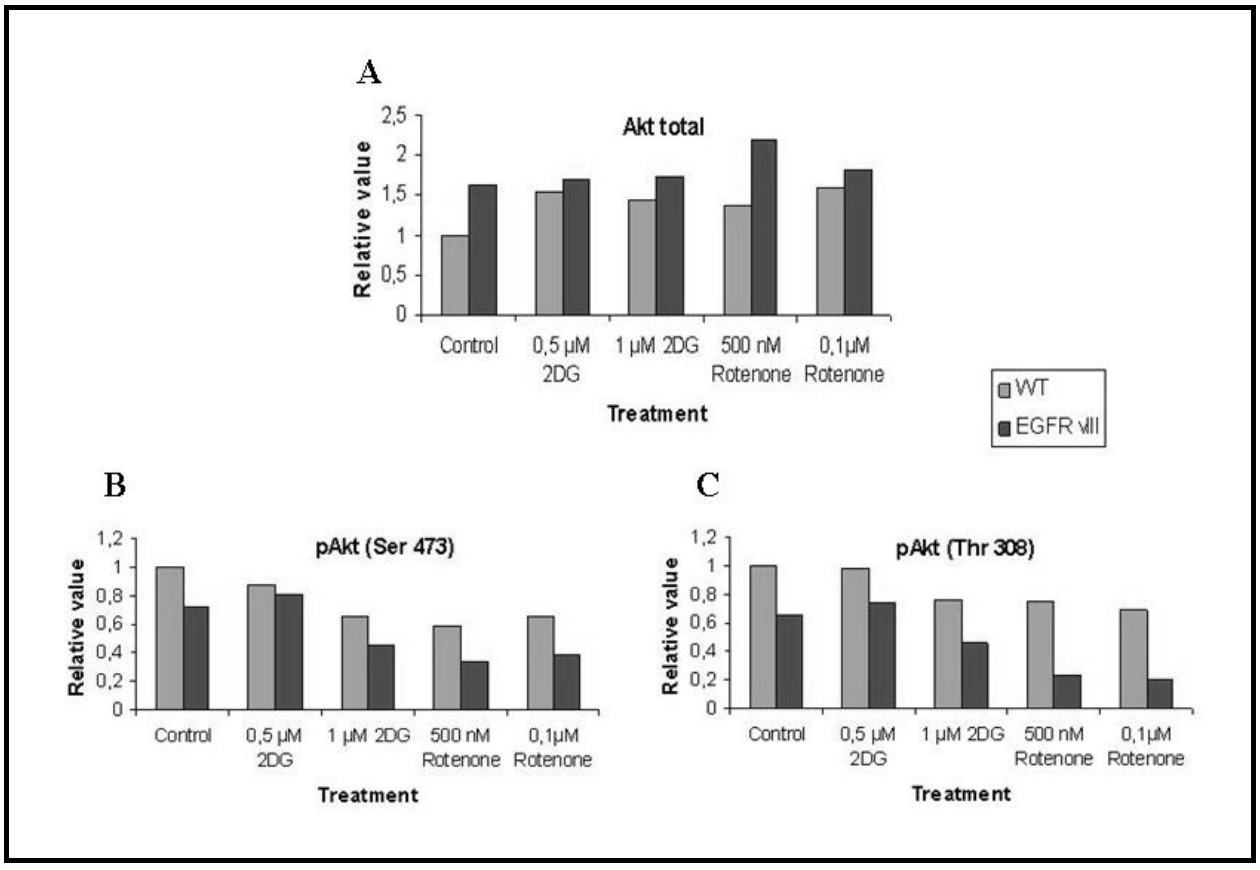

Figure 8.13. Expression and activation of Akt in fixated U87 WT and EGFR vIII cells. The cells were grown in a culture flask for 24 hours before treated for another 24 hour with rotenone or 2DG. During this time the flasks were incubated at 37°C/5% CO_2 in a cell incubator. Furthermore, the cells were fixated using 3.7% formaldehyde. Measurements were carried out using three different primary antibodies, anti-Akt (total), anti-phospho-Akt (Ser 473) and anti-phospho-Akt (Thr 308). $0.5 \cdot 10^6$ cells were used for each sample and one antibody was measured at the time. The primary antibodies were added to a final concentration of 1:100. After a 60 minutes incubation time, a secondary antibody was added to each sample before measured using a BD FACSCalibur™ flow cytometer. The presented data are normalized relative to the WT control.

Akt expression and phosphorylation

The pro-survival Akt protein is often found to be overexpressed in malign cells. By staining specific antibodies for the Akt phosphorylation sites we could assess how much of the expressed protein was phosphorylated.

As seen in figure 8.13, after one day of rotenone and 2DG treatment, the Akt level was 1.6 fold higher in EGFR vIII cells compared to WT cells. However, the Akt expression was increased in both 2DG and rotenone treated WT cells. The Akt levels after 2DG treatment were similar in the two different cell lines, since EGFR vIII cells remained unchanged. On the other hand, rotenone tended to increase the Akt expression in the EGFR vIII cells as well. The most elevated Akt expression is seen for the EGFR vIII cells treated with 500nM rotenone. Here a 1.6 fold increase compared to the WT cells is seen.

To be activated, Akt depend on phosphorylation at its two phosphorylation sites, the regulatory domain at serine 473 and the kinase domain at threonine 308. Despite an elevated Akt expression the amount of active Akt decreases as seen in figure 8.13 B and C. Overall the WT cell line contain more phosphorylated Akt than the EGFR vIII. The two cell lines respond similarly to 2DG treatment, and displayed a dose dependent tendency of decrease in Akt phosphorylation at both Ser 473 and Thr 308. Although rotenone also gave reduced phosphorylation at these sites in both cell lines, the response was more pronounced for the Akt Thr 308 site in the EGFR vIII cells. This may indicate regulatory changes in these cells.

AMPK expression and phosphorylation

AMPK is a protein working as a sensor of cellular energy, and is activated upon nutrient deprivation, low energy status and stress. The protein is a heterotrimer and depends on all the three subunits α, β and γ for activation.

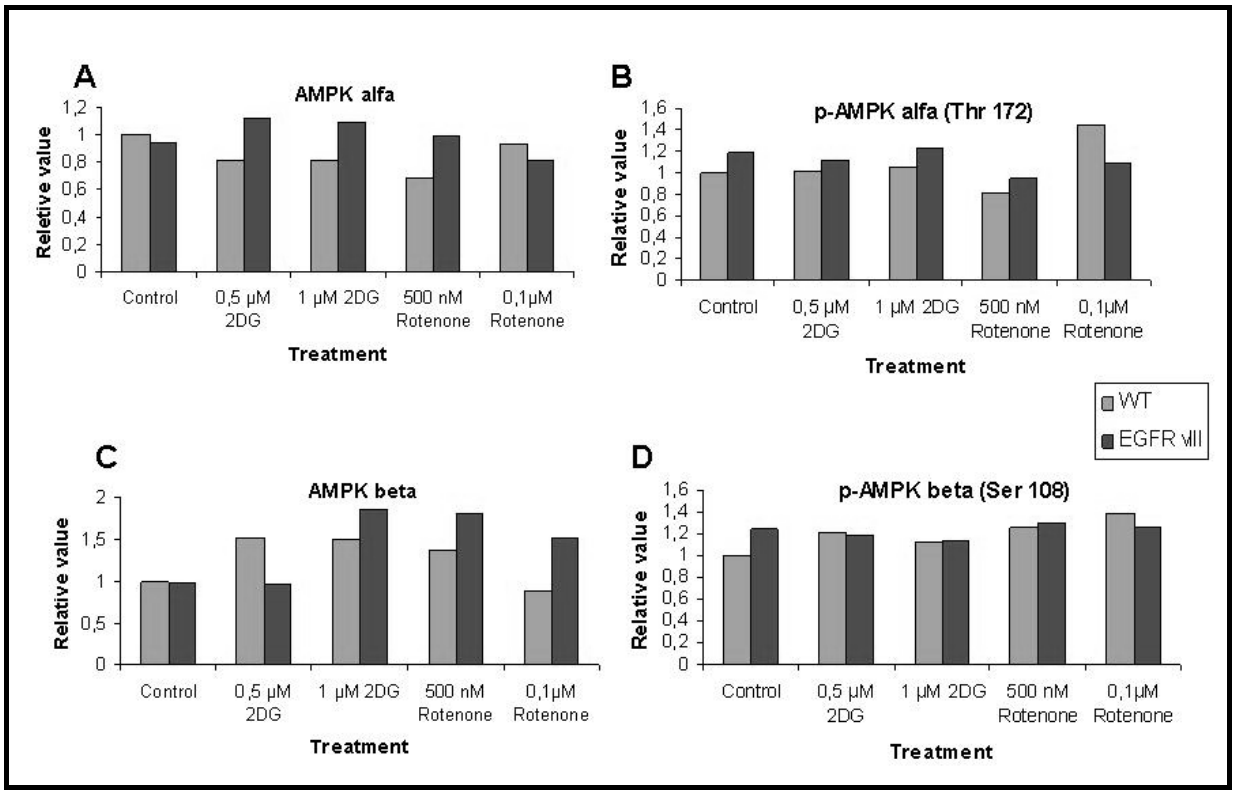

Figure 8.14. Expression and activation of AMPK α/AMPK β in fixated U87 WT and EGFR vIII cells. The cells were grown in a culture flask for 24 hours before treated for another 24 hour with rotenone or 2DG. During this time the flasks were cultured at 37°C/5% CO_2 in a cell incubator. Furthermore, the cells were fixated using 3.7% formaldehyde. Measurements were carried out using four different primary antibodies, anti-AMPK α, anti-phospho- AMPK α (Thr 72), anti-AMPK β and anti-phospho-AMPK β (Ser 108). $0.5 \cdot 10^6$ cells were used for each sample and one antibody was measured at the time. The primary antibodies were added to a final concentration of 1:50 (1:100 for the anti-phospho-AMPK β (Ser 108) antibody). After a 60 minutes incubation time, a secondary antibody was added to each sample before measured using a BD FACSCalibur™ flow cytometer. The presented data are normalized relative to the WT control.

From the experiment where the expressions of the catalytic AMPK α subunit were measured, minor differences were observed. Compared to the WT control cell line the AMPK α expression was slightly higher for the 2DG treated EGFR vIII cells, while a decreased phosphorylation was seen in WT cells treated with 2DG and low concentration (0.1µM) rotenone.

Examination of the phosphorylation site at the AMPK α subunit indicates the activation state of the subunit. According to our observations (Figure 8.14), 2DG did not affect AMPK α activation. When treated with low rotenone concentrations (500nM) a minor drop in Thr 172 phosphorylation was observed for both cell lines. A 1.4 fold increase in AMPK α activation was seen for the 0.1µM rotenone treated WT cells while the EGFR vIII showed similar properties as the control cells.

Furthermore, expressions of the glycogen binding AMPK β subunit were measured. As shown in Figure 8.14 C, the treated cells had a similar or raised expression of the subunit compared

to control cells. EGFR vIII cells had an elevated expression of the subunit after treatment with 1µM 2DG or rotenone. Especially after rotenone treatment, the effect was more pronounced in the EGFR vIII cells.

As our previous data on AMPK α activation, the amount of activated AMPK β were at similar levels in the two cell types, and remained unchanged after the treatments.

ACC expression and phosphorylation

ACC is a regulator of fatty acid oxidation and is located downstream of AMPK in the metabolic cascade. AMPK phosphorylation increases the phosphorylation of ACC and deactivates it enzymatic activity.

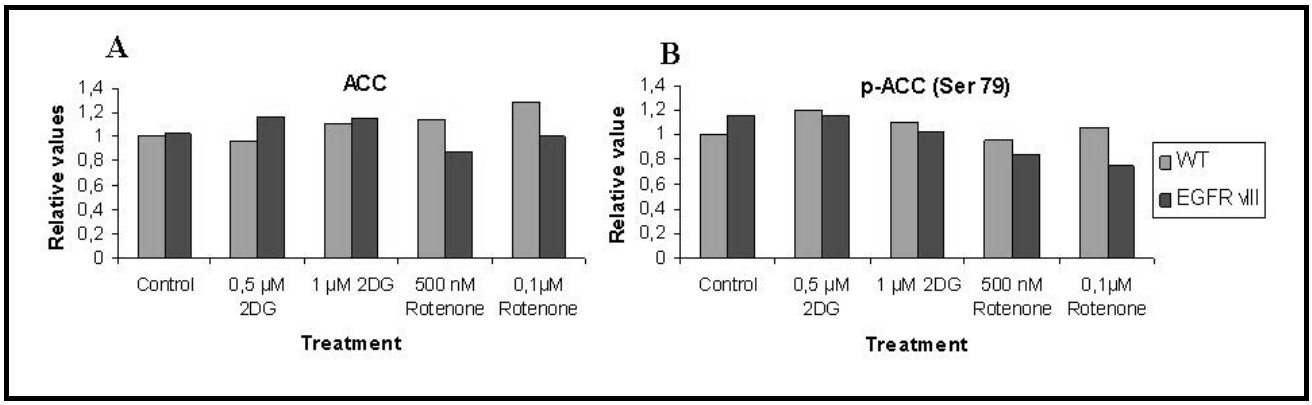

Figure 8.15. Expression and activation of ACC in fixated U87 WT and EGFR vIII cells. The cells were grown in a culture flask for 24 hours before treated for another 24 hour with rotenone or 2DG. During this time the flasks were kept at 37°C/5% CO_2 in a cell incubator. Furthermore, the cells were fixated using 3.7% formaldehyde. Measurements were carried out using two different primary antibodies, anti-ACC and anti-phospho-ACC (Ser 79). $0.5 \cdot 10^6$ cells were used for each sample and one antibody was measured at the time. The primary antibodies were added to a final concentration of 1:400 for the anti-ACC and 1:25 for the anti-phospho-ACC (Ser 79). After a 60 minutes incubation time, a secondary antibody was added to each sample before measured using a BD FACSCalibur™ flow cytometer. The presented data are normalized relative to the WT control.

The untreated WT and EGFR vIII cells have similar ACC expression and phosphorylation properties due to our observations. These findings also demonstrated that the expression and activation of ACC in the glioma cells were unaffected by 2DG and rotenone treatment (Figure 8.15 A and B).

8.8 Use of fluorescent probes to determine mitochondrial properties

Our experiments on protein signalling and metabolic regulation showed some variations between the two cell lines. Therefore, we wanted to look for correlations between our previous results and mitochondrial properties that are often affected in cancer cells. The

characteristics investigated were mitochondrial mass, mitochondrial membrane potential and ROS production.

NAO - Nonyl Acridine Orange

NAO binds selectively to the cardilipin lipid in the inner mitochondrial membrane and can be used for determination of mitochondrial mass within cellular samples.

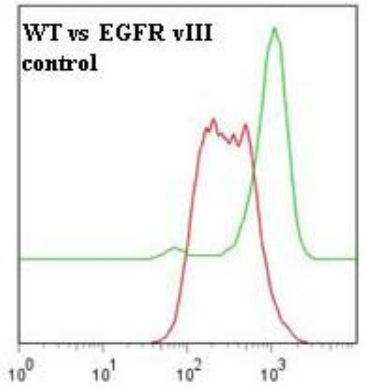

A.

Sample name	Geometric mean, FL1	Frequency of total
EGFR vIII control	862,64	0,79
WT control	284,40	0,91

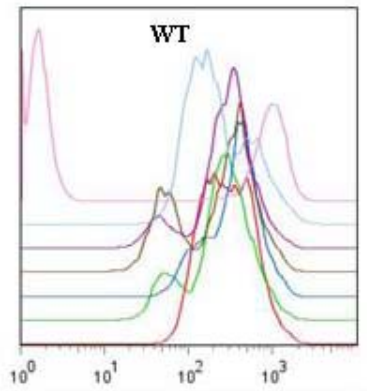

B.

Samplename	Geometric mean, FL1	Frequency of total
WT autofluorescence	27,94	0,93
WT FCCP	227,19	0,95
WT 0,1µM rotenone	260,75	0,96
WT 500nM rotenone	206,67	0,96
WT 1µM 2DG	329,15	0,92
WT 0,5µM 2DG	233,05	0,97
WT control	284,40	0,91

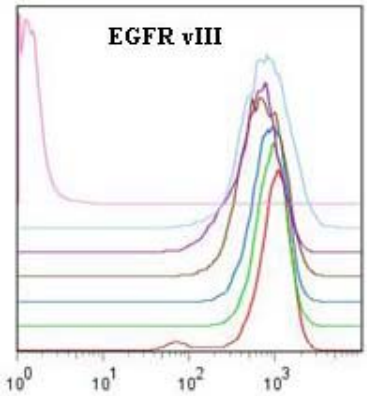

C.

Samplename	Geometric mean, FL1	Frequency of total
EGFR vIII autofluorescence	1,45	0,96
EGFR vIII FCCP	747,00	0,85
EGFR vIII 0,1µM rotenone	563,61	0,84
EGFR vIII 500nM rotenone	675,26	0,78
EGFR vIII 1µM 2DG	819,43	0,71
EGFR vIII 0,5µM 2DG	877,14	0,86
EGFR vIII control	862,64	0,79

Figure 8.16. Results from NAO measurements of rotenone and 2DG treated cells. The cells were grown in a culture flask for 24 hours before treated for another 24 hour with rotenone or 2DG. During this time the flasks were incubated at 37°C/5% CO_2 in a cell incubator. NAO was added to $0.5 \cdot 10^6$ cells to a final concentration of 200nM. As a control FCCP was added to one of the samples to a final concentration of 0,2mM. Fluorescent measurements were carried out at a BD FACSCalibur™ Flow Cytometer and detected in FL-1 **(A)** NAO stained control cells for WT and EGFR vIII **(B)** NAO stained WT cells **(C)** NAO stained EGFR vIII cells.

The measured mitochondrial mass for the untreated control cells are shown in figure 8.16 A. Here, the presented findings suggest a higher content of mitochondria in EGFR vIII cells compared with WT cells.
The treated WT cells have an elevated mitochondrial mass compared to the control cells according to the results presented in figure 8.16 B (when comparing the geometric mean values). The curves indicate a possible bimodal cell population within the WT cell line, and must be investigated in more detail. Here EGFR vIII cells show a different behaviour (Figure 8.16 C). The 2DG treated cells have an unaffected mitochondrial mass while a decreased mitochondrial content are observed for the rotenone treated EGFR vIII cells.

TMRM - Tetramethyl Rhodamine Methyl Ester

The most common probe used to determine mitochondrial membrane potential ($\Delta\Psi m$) is the fluorescent probe TMRM.
In this experiment we observed an enhanced $\Delta\Psi m$ in untreated EGFR vIII control cells when compared to the WT control (Figure 8.17 A). Here, the geometric mean values of the mutated control are approximately twice as high as the WT. Using these data from Figure 8.17 B and C, we observed that the $\Delta\Psi m$ for both cell lines were unaffected by metabolic inhibitors. The uncoupler FCCP was also added as a control of low membrane potential. This addition did not have the desirable effect, maybe because the FCCP concentration was to low.

ROS - CM_2H_2DCFDA

ROS are implicated in cell signalling and metabolism, and are considered to play major roles as carcinogens. The mitochondria are major producers of ROS within the cells, and we here wanted to measure ROS levels using CM_2H_2DCFDA as detecting probe.
As seen in figure 8.18 A, our measurements indicate possible differences in ROS concentrations between the two cell lines. From the geometric mean calculations we can see elevated ROS concentration within the EGFR vIII cells compared to the WT. When treated with 2DG the WT cell line have an increased ROS production, while rotenone treatment does not have an obvious effect on ROS (Figure 8.18 B). Upon rotenone treatment, the ROS production in EGFR vIII cells decreases with elevated rotenone concentration. A minor reduction in ROS concentration is also seen for the 2DG treated EGFR vIII cells (Figure 8.18 C).

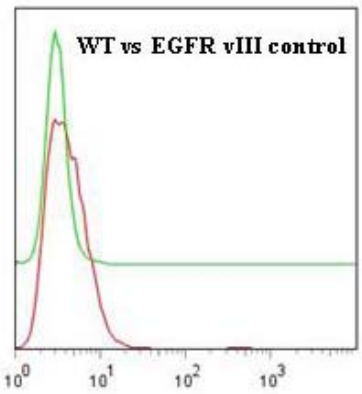

A.

Sample name	Geometric mean, FL2	Frequency of total
EGFR vIII control	74,05	0,94
WT control	50,68	0,95

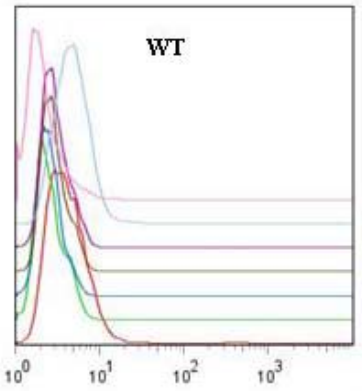

B.

Sample name	Geometric mean, FL2	Frequency of total
WT autofluorescence	13,48	0,92
WT FCCP	49,50	0,94
WT 0,1µM rotenone	56,65	0,91
WT 500nM rotenone	52,15	0,95
WT 1µM 2DG	49,42	0,91
WT 0,5µM 2DG	40,69	0,96
WT control	50,68	0,95

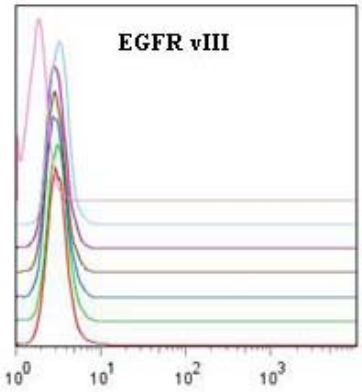

C.

Sample name	Geometric mean, FL2	Frequency of total
EGFR vIII autofluorescence	1,34	0,93
EGFR vIII FCCP	68,96	0,93
EGFR vIII 0,1µM rotenone	75,67	0,90
EGFR vIII 500nM rotenone	73,08	0,92
EGFR vIII 1µM 2DG	68,78	0,95
EGFR vIII 0,5µM 2DG	74,30	0,94
EGFR vIII control	74,05	0,94

Figure 8.17. Measurements of mitochondrial membrane potential (ΔΨm) in rotenone and 2DG treated cells. The cells were grown in a culture flask for 24 hours before treated for another 24 hour with rotenone or 2DG. During this time the flasks were kept at 37°C/5% CO_2 in a cell incubator. TMRM were added to $0.5 \cdot 10^6$ cells to a final concentration of 200nM. As a control FCCP was added to one of the samples to a final concentration of 0,2mM. Fluorescent measurements were carried out at a BD FACSCalibur™ Flow Cytometer and detected in FL-2. **(A)** TMRM stained control cells for WT and EGFR vIII **(B)** TMRM stained WT cells **(C)** TMRM stained EGFR vIII cells.

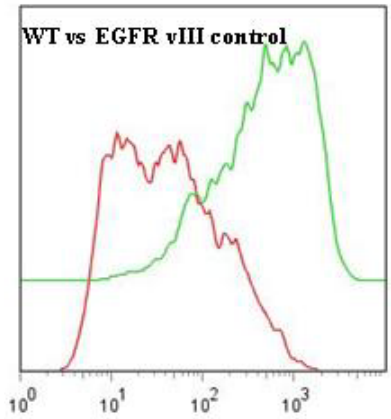

A.

Sample name	Geometric mean, FL1	Frequency of total
EGFR vIII control	453,78	0,91
WT control	41,65	0,95

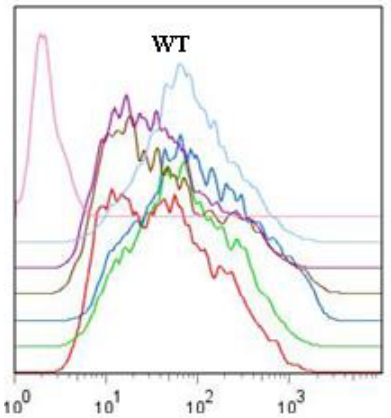

B.

Samplename	Geometric mean, FL1	Frequency of total
WT autofluorescence	2,21	0,93
WT H_2O_2	77,46	0,93
WT 0,1µM rotenone	37,38	0,93
WT 500nM rotenone	48,80	0,93
WT 1µM 2DG	103,54	0,95
WT 0,5µM 2DG	68,38	0,94
WT control	41,65	0,95

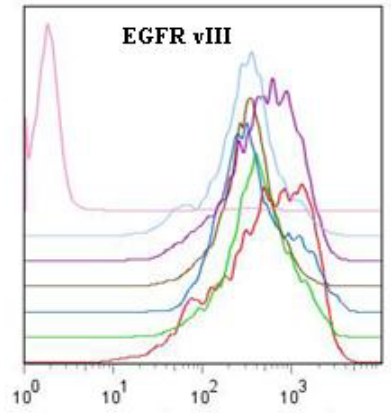

C.

Samplename	Geometric mean, FL1	Frequency of total
EGFR vIII autofluorescence	2,19	0,92
EGFR vIII H_2O_2	289,57	0,91
EGFR vIII 0,1µM rotenone	463,66	0,91
EGFR vIII 500nM rotenone	308,32	0,92
EGFR vIII 1µM 2DG	378,11	0,93
EGFR vIII 0,5µM 2DG	405,70	0,90
EGFR vIII control	453,78	0,91

Figure 8.18. Measurements of ROS concentrations in rotenone and 2DG treated cells. The cells were grown in a culture flask for 24 hours before treated for another 24 hour with rotenone or 2DG. During this time the flasks were incubated at 37°C/5% CO_2 in a cell incubator. CM_2H_2DCFDA was added to $0.5 \cdot 10^6$ cells to give a final concentration of 5µM. As a control H_2O_2 was added to one of the samples to a final concentration of 100µM. . Fluorescent measurements were carried out at a BD FACSCalibur™ Flow Cytometer and detected in FL-1.
(A) ROS stained control cells for WT and EGFR vIII **(B)** ROS stained WT cells **(C)** ROS stained EGFR vIII cells.

9. Discussion

The aim of the study was to determine if EGFR mediated signalling represents a possible regulatory link between cellular proliferation and energy metabolism. This theory was investigated by comparing a cell line having constitutively active EGFR signalling with wild type cells. The cells were challenged with selective modulators of energy metabolism, and several characteristics describing physiological and biochemical properties were analysed.

Our data indicate possible metabolic variations between the cell lines, with the WT cells having an elevated respiratory capacity while the EGFR vIII cells show an enhanced glycolysis, which is consistent with the level of aggressiveness for the two cell lines [14, 15]. Mitochondrial characteristics such as mitochondrial mass, mitochondrial membrane potential and ROS production also seem to be raised for the mutated cells. No distinct difference in proliferation properties were observed for the two cell lines under normal cellular conditions. Upon energy deprivation, rotenone treatment had a stronger inhibitory effect on proliferation in EGFR vIII cells, while 2DG treatment had a similar effect on EGFR vIII and WT respectively. This study also discovered possible difference in cellular stress response and intracellular signalling.

When characterizing the cells we measured the occurrence of mutated EGFR vIII protein within the two cell lines to ensure a difference in protein expression. By the use of flow cytometry and western blot analysis we confirmed over-expression of the EGFR vIII protein in the mutated cells compared to the WT. These methods are well established to confirm protein expression [64]. An advantage with flow cytometry is that it is less time consuming compared to a western blot. Western blotting on the other hand represents a more specific antibody binding.

The three proliferations assays used in this study, BrdU, alamarBlue and MTT, use distinct cellular characters to determine cellular proliferation. BrdU measures cellular DNA synthesis by incorporating into the cellular DNA, whereas the alamarblue and MTT assays are based on different metabolic activities within living cells [65]. As cell characteristics may be disturbed upon gene manipulation [1], an absolute correlation can not be expected between the assays. This was observed in our experiments where some differences between the proliferation

assays were seen. The MTT assay indicated that the WT cells had a higher proliferation rate compared to the mutated EGFR vIII cell line, However, BrdU incorporation showed an enhanced proliferation for the EGFR vIII cells compared to WT. The final assay, alamarblue, resulted in similar proliferation properties for both the mutated and the WT U87 cells. All the three proliferation assays presents a higher proliferation rate for the U87 glioma cells than the 3T3 reference cell line. These findings correlate to the fact that highly aggressive malignant cells have an abnormal proliferation compared to transformed cells [14]. Our results suggest that care should be taken when choosing proliferation assay, which is in line with previous observations [66].

Our data demonstrated a possible aberrant interaction between the MTT assay reactants and metabolic modulators such as rotenone (Figure 8.9). MTT is therefore an unsuitable assay for detecting proliferation properties in rotenone treated cells. A significant analytical variance was seen, and the lack of effect of rotenone was unexpected and not in correlation with the BrdU assay. Findings suggest that the MTT itself may affect cellular functions and conditions to some extent, causing some discordance of cell viability measurement [67]. This could be the fact, but at the same time our data on untreated cells seemed to correlate to the other proliferation assays. A possible explanation for these effects can be an interaction between rotenone and the MTT reaction system. Rotenone is an inhibitor of complex I in the ETC, while MTT has been suggest to be mainly reduced bymitochondrial, microsomal and cytosolic enzymes [68]. The MTT reduction process is not fully understood, and potentially mitochondrial reductases, such as complex I, can be involved in the reaction which can explain the possible interactions with rotenone [69]. It has been postulated that changes in metabolic activity can give large changes in MTT results even if the number of viable cells is constant [70].
Since alamarblue reduction is believed to be mediated, at least in part, by mitochondrial enzymes, the proliferation assay was excluded from further experiments on rotenone treated cells [71]. The data from the three assays did not suggested dramatic differences in proliferation between the two cell types. Based on the above discussion the BrdU assay was chosen in the following experiments.

According to our results, the WT and 3T3 cells were more resistant to rotenone than the mutated cell line (Figure 8.10). EGFR vIII immediately responded to the added rotenone shown by a rapid decrease in cell proliferation, while higher rotenone concentrations are

needed to obtain the same effect in the WT and 3T3 cell line. According to our respiratory data the WT cell line had a higher routine respiration than EGFR vIII cells (Figure 8.5). Consequently we believed that the WT cells would be more affected by the respiratory blockage caused by rotenone. As this effect was not observed we hypothesise that the WT U87 glioma cells are capable of turning to glycolysis when respiratory energy is absent [72]. The fact that the EGFR vIII mitochondria show a more rotenone sensitive behaviour may indicate that the mutated cells lack the metabolic flexibility present in WT cells.

Glycolytic blockage by 2DG produced a similar response in WT and mutated cells. In our findings we observed a raised lactate secretion for EGFR vIII cells, indicating an elevated glycolysis. 2DG inhibition has been reported to induce Akt phosphorylation at Thr 308 and to induce oxidative stress caused by ROS [73]. Being kept in a glucose rich culture media, glucose is the main nutrient source for the proliferating cells. Therefore, by blocking the glycolysis the pyruvate production needed for driving the citric acid cycle is inhibited [4]. As the citric acid cycle is the main supplier of NADH and succinate to the ETC, 2DG treatment will affect the ETC in an indirect manner. This effect could possibly be avoided by growing the cells in fat rich medium. Here, fatty acid oxidation would supply acetyl CoA to the citric acid cycle, and at the same time the actual glycolytic inhibition by 2DG could be measured.

The EGFR vIII cell line appeared to have a lower respiratory reserve capacity (coupling), as shown by our oxygraph measurements (figure 8.5). This tells us that WT cells may have a higher respiratory potential that can be used when exposed to stress, while EGFR vIII, which under normal conditions, use respiration closer to its max capacity may be more sensitive to additional stress. Despite the variation in respiratory status, both WT and EGFR vIII seem to utilize both respiratory and glycolytic energy production to maintain their cellular ATP homeostasis. Protein expression patterns can govern this modulation ability as shown and reviewed in other studies [74, 75].

The aggressive tumor behaviour of EGFR vIII is presented by elevated proliferation, increased tumor volumes, down regulated apoptosis and a decreased response to therapeutically treatment compared to the WT cell line [76]. The increased lactate secretion seen within EGFR vIII cells support our respiratory findings. Lactate is a natural by-product of glycolysis under anaerobic conditions. However, highly glycolytic cancer cells secrete elevated levels of lactate even under aerobic conditions [14]. Measuring lactate secreted by

the cells gave us an indication of the glycolytic activity within the two cell lines. Based on our results the mutated cell line is more dependent on the glycolysis for energy production, while WT cells use mitochondrial respiration to a greater extent. These results correspond to the fact that aggressive cancers have raised glucose consumption [77].
Our investigation of mitochondrial morphology indicates a filamentous mitochondrial network surrounding the nucleus in both cell types (figure 8.3). These preliminary experiments do not indicate that there is a change in mitochondrial localization or morphology upon EGFR vIII over-expression, however further analysis have to be made to confirm these results.

Mitochondrial mass was measured using NAO which binds to cardiolipin in the mitochondrial matrix. Our experiment indicates an elevated mitochondrial content within EGFR vIII control cells compared to WT (Figure 8.16 A). Even if a higher mitochondrial level in was found EGFR vIII, this was not clear by the mito-tracker imaging. An extensive examination of mitochondrial biogenesis is needed to reveal a possible aberration [78].

The NAO signal in 2DG treated EGFR vIII cells were unaffected compared to control, while it decreased for rotenone treated cells. As previously stated the mitochondria in EGFR vIII cells may have a reduced ETC capacity. The cells may try to make up for this by increasing mitochondrial biogenesis, giving a raised mitochondrial mass in mutated cells [79]. Impaired mitochondria can produce high levels of ROS [80], and by inducing more stress by rotenone treatment these mitochondria might reach a threshold where they are targeted for active degradation, so called mitophagy [81]. This is an active process in which damaged mitochondria are selectively removed from the cell by autophagy [81]. This can explain the decrease in NAO signal from rotenone treated EGFR vIII cells. These results correlate with the increased ROS production seen in EGFR vIII. Changes in EGFR vIII mitochondria may thus increase mitochondrial ROS production and thereby make these cells more sensitive for metabolic stress. Based on these results, we hypothesize that EGFR vIII contain a high number of deficient mitochondria, therefore production of ROS could be significantly increased upon rotenone treatment. Furthermore, the oxygraph measurements showed a reduced respiratory reserve capacity of the EGFR vIII cells compared to WT cells. These findings may also occur due to an increased number of deficient mitochondria in the mutated EGFR vIII cell line and strengthens the mitophagy hypothesis.

Under normal conditions ROS operates as intracellular signalling molecules [82]. High levels of ROS can be damaging to cellular compounds such as lipids, DNA and proteins [80]. Complex I and III in the ETC have been suggested to be the major ROS source in the mitochondria, and this ROS can readily influence the mitochondrial function [12].
Our studies indicate an elevated ROS production in the mutated EGFR vIII cells (Figure 8.18). When examining the EGFR vIII cell line a decreased ROS production was seen upon rotenone treatment. A possible explanation for this behaviour can be the fact that ETC inhibition reduces ROS generation as have been suggested by previous studies [83]. Another possibility in ROS decrease can be due to mitophagy [81]. In EGFR vIII control cells the mitochondria may be damaged (due to mutations) and produce ROS, but are still operative enough to supply the cells with small amounts of ATP. When rotenone is added the mitochondria are pushed into an un-functional state where the cells decide to degrade the damaged mitochondria by mitophagy, hence leading to a reduced ROS production.

Our findings indicate a higher mitochondrial membrane potential ($\Delta\Psi m$) for the EGFR vIII cells compared to control, and in both cell lines the $\Delta\Psi m$ was unaffected by 2DG and rotenone treatment compared to their respective controls. $\Delta\Psi m$ reflects ETC activity and mitochondrial function [84], but when adding rotenone no major difference was seen. Studies have shown that cells with an enhanced intrinsic $\Delta\Psi m$ are better at handling hypoxia, avoiding apoptosis, initiate angiogenesis, show good growth properties under though conditions and have raised basement membrane invading properties [9]. Despite the fact that our experiments indicated similar proliferation properties for WT and EGFR vIII, these properties might change *in vivo*.

The Akt protein is often overexpressed in malign cells where it among other properties acts as a stimulator of glycolysis and an inducer of apoptotic resistance [33].
Our study shows a higher expression of Akt for the EGFR mutated cells, especially under normal conditions. This may suggest that the EGFR vIII cells have increased survival signalling, but at the same time they are metabolically less flexible and therefore more sensitive to energetic stress induced by rotenone. As the cells are treated with reagents blocking their nutrient supply, they become more dependent on pro survival stimuli for survival [85]. Lacking the extracellular binding domain, the EGFR vIII has been suggested to be constantly activated leading to an increased activation of the Akt pathway [60].

In order to achieve its activated state, the two Akt phosphorylation sites (Ser 473 and Thr 308) must be phosphorylated [41]. We observed a decreased phosphorylation status for the treated cells when compared to control, and this indicates a reduced Akt activation. WT cells have a higher Akt phosphorylation compared to EGFR vIII where Akt is almost knocked down.
Upon Akt activation the regulatory domain Ser 473 is first phosphorylated while the phosphorylation of the Thr 308 kinase domain occurs second to the Ser 473 activation [41]. This is reflected in the phosphorylation patterns we observed from our anti-phospho flow experiment for these two phosphorylation sites.

There seem to be a mechanism for raising the protein expression of Akt when the cells are treated with 2DG or rotenone, but according to the phosphorylation data less Akt is active. The protein Akt may be upregulated but not activated via phosphorylation. This could be a way for the cells to prepare itself for a scenario of enhanced stress.
Akt expression is upregulated in EGFR vIII when treated with low rotenone concentrations, whereas the upregulation is lower in cells treated with high rotenone concentration. Damaged mitochondria produce ROS, but severely damaged mitochondria can be removed by mitophagy [81]. This could be the case here, where the high rotenone concentration triggers the mitophagy pathway and removes the detrimental mitochondria. Moreover it has been shown that ROS suppresses Akt activity [86] which correlates with our findings that EGFR vIII cells with high amount of ROS have less Akt activation.

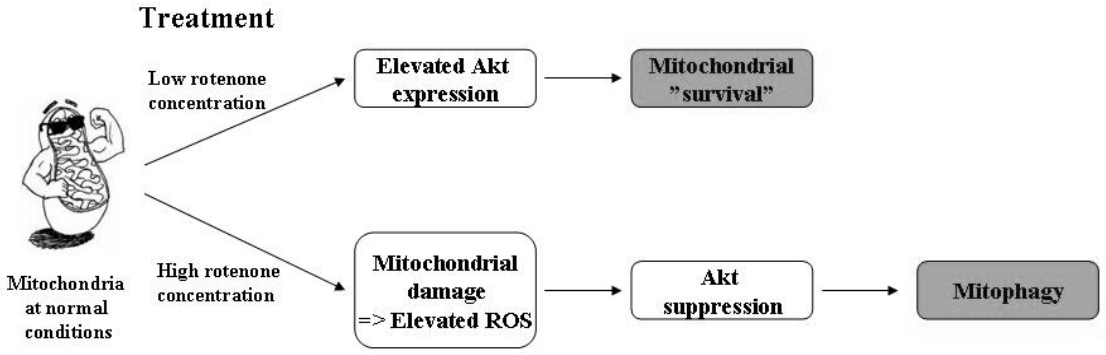

Figure 9.1 Suggested model of mitochondrial responses to treatment with energy suppressors.

AMPK is a protein acting as a sensor for cellular energy status and is activated by nutrition deprivation and stress. The activated AMPK reconfigures the cellular metabolism from an energy consuming to an energy saving state [13]. AMPK is made up of three subunits with

the α-subunit being catalytic, the β-subunit containing a glycogen sensing domain and the γ-subunit having AMP/ATP binding capacity [13]. In our experiments the expression and activity of the two AMPK subunits α and β were measured. Treatment with 2DG and rotenone had little or no effect on AMPK α protein expression. However, at the phosphorylation site Thr 172 of AMPK α, rotenone treatment gave a change in phosphorylation.
For AMPK β, a slightly different expression pattern was seen. Here, the rotenone and 2DG treated cells present elevated protein levels.According to the Ser 108 phosphorylation site just a small increase in AMPK β activity is seen for the treated cells. The protein expression of AMPK β has a similar pattern as Akt, but under stress conditions a fall in Akt phosphorylation is seen while a minor raise in AMPK β activation occur. This behaviour can be explained from Figure 5.7 where Akt is seen to be an upstream inhibitor of AMPK. These findings correlate with previous experiments onMDA-MB-468 breast cancer cells [85].

ACC is a downstream enzyme of AMPK regulating the oxidation of fatty acids. Active AMPK phosphorylate and inactivates metabolic enzymes such as ACC [87].
According to our findings, the ACC expression and activation is unaffected by 2DG and rotenone treatment. These results correspond to the findings of activated AMPK where minor changes in AMPK activation were seen. ACC staining was utilized as an indicator of AMPK activation [85] and a possible mismatch between AMPK and ACC activation could reveal experimental errors.

Enhanced glycolytic activity is followed by high pyruvate concentrations and increased lactate production [3]. Under conditions where the energy supply is blocked, cells are forced to modify their metabolism in order to survive. From our measurements using 2DG and rotenone, different metabolic properties for WT and EGFR vIII were seen. EGFR vIII was most inhibited by 2DG treatment, while rotenone treatment gave a raised lactate secretion within both cell lines. These findings correlate to the hypothesis that aggressive tumors have an upregulated glycolysis [77]. The fact that WT cells are more resistant to 2DG may indicate that WT cells are more capable of switching between glycolysis and mitochondrial respiration as its main nutrient source. Under the given growth conditions WT seem to be better suited for survival compared to the EGFR vIII which has a higher dependence on glycolytic energy production.

10. Conclusions and future perspectives

The results obtained from this study indicate different mitochondrial properties for U87 glioma WT and EGFR vIII cells. The cell line containing the mutated EGFR vIII protein has previously been proven to present a more aggressive behaviour than the WT cell line. This statement correlate with our findings as an increased glycolytic activity and a decreased mitochondrial respiration within the EGFR vIII cells were observed. These characteristics are known to be hallmarks for aggressive cancer cells.
Despite these metabolic modifications no obvious difference in proliferational behaviour were observed between the cell lines. This may be due to the fact that EGFR vIII have favorable properties within *in vivo* growing tumors [88], properties that are not present under these *ex vivo* given growth conditions. Therefore, a different proliferation pattern may have been found if the cells had been grown as spheroids or under *in vivo* conditions.
EGFR vIII cells were found to be more sensitive to respiratory inhibition and we therefore suggest a possible defect in the respiratory system for this cell line. These findings were strengthend by our results showning elevated mitochondrial mass and ROS production within EGFR vIII cells. We hypothesize that to make up for the disturbed mitochondrial ATP production the cells elevate their mitochondrial biogenesis. This creates an enhanced production of ROS which may further damage the mitochondrial function. If the mitochondrial damage is too extensive, the unfunctional mitochondria can be degraded by mitophagy.
We also found that upon energy blockage the U87 cells express higher levels of Akt and AMPKβ. A decreased phosphorylation for Akt was measured and this may also support our thesis as raised ROS concentration is a suppressor of Akt activity.

The results in this study are based on data from a limited number of experiments, and some of the experiments will have to be repeated and/or expanded in order to be able to draw more firm conclusions.
An exciting future objective would be to examine if EGFR vIII cells are more capable of modulating their metabolism when treated with a combination of glycolytic and respiratory inhibitiors than the WT cell line.
To increase our knowledge on the metabolic role of EGFR vIII, we must examine other possible contributors in the metabolic regulatory system. Interesting targets for futher analysis

will be the protein synthesis regulator mTOR, the tumor suppressor p53 or the Ras-Raf-MEK-ERK and JAK/STAT transcriptional pathways.

To increase our understanding on mitochondrial dysfunction in cancer cells and their role in metabolic regulation, further studies must be carried out. A goal for the future must be to identify metabolic targets that can be used for clinical treatment.

11. References

1. Hanahan, D. and R.A. Weinberg, *The hallmarks of cancer.* Cell, 2000. **100**(1): p. 57-70.
2. Ristow, M., *Oxidative metabolism in cancer growth.* Curr Opin Clin Nutr Metab Care, 2006. **9**(4): p. 339-45.
3. Racker, E., *History of the Pasteur effect and its pathobiology.* Mol Cell Biochem, 1974. **5**(1-2): p. 17-23.
4. Moreno-Sanchez, R., S. Rodriguez-Enriquez, A. Marin-Hernandez, and E. Saavedra, *Energy metabolism in tumor cells.* FEBS J, 2007. **274**(6): p. 1393-418.
5. Bianchi, N.O., M.S. Bianchi, and S.M. Richard, *Mitochondrial genome instability in human cancers.* Mutat Res, 2001. **488**(1): p. 9-23.
6. Modica-Napolitano, J.S., M. Kulawiec, and K.K. Singh, *Mitochondria and human cancer.* Curr Mol Med, 2007. **7**(1): p. 121-31.
7. Grossman, L.I. and E.A. Shoubridge, *Mitochondrial genetics and human disease.* Bioessays, 1996. **18**(12): p. 983-91.
8. Baysal, B.E., R.E. Ferrell, J.E. Willett-Brozick, E.C. Lawrence, D. Myssiorek, A. Bosch, A. van der Mey, P.E. Taschner, W.S. Rubinstein, E.N. Myers, C.W. Richard, 3rd, C.J. Cornelisse, P. Devilee, and B. Devlin, *Mutations in SDHD, a mitochondrial complex II gene, in hereditary paraganglioma.* Science, 2000. **287**(5454): p. 848-51.
9. Heerdt, B.G., M.A. Houston, and L.H. Augenlicht, *Growth properties of colonic tumor cells are a function of the intrinsic mitochondrial membrane potential.* Cancer Res, 2006. **66**(3): p. 1591-6.
10. Schatz, G., *The protein import system of mitochondria.* J Biol Chem, 1996. **271**(50): p. 31763-6.
11. Jezek, P., H. Engstova, M. Zackova, A.E. Vercesi, A.D. Costa, P. Arruda, and K.D. Garlid, *Fatty acid cycling mechanism and mitochondrial uncoupling proteins.* Biochim Biophys Acta, 1998. **1365**(1-2): p. 319-27.
12. Turrens, J.F., *Superoxide production by the mitochondrial respiratory chain.* Biosci Rep, 1997. **17**(1): p. 3-8.
13. Towler, M.C. and D.G. Hardie, *AMP-activated protein kinase in metabolic control and insulin signaling.* Circ Res, 2007. **100**(3): p. 328-41.
14. Gatenby, R.A. and R.J. Gillies, *Why do cancers have high aerobic glycolysis?* Nat Rev Cancer, 2004. **4**(11): p. 891-9.
15. Warburg, O., *On respiratory impairment in cancer cells.* Science, 1956. **124**(3215): p. 269-70.
16. Vogelstein, B. and K.W. Kinzler, *The multistep nature of cancer.* Trends Genet, 1993. **9**(4): p. 138-41.
17. Kelloff, G.J., J.M. Hoffman, B. Johnson, H.I. Scher, B.A. Siegel, E.Y. Cheng, B.D. Cheson, J. O'Shaughnessy, K.Z. Guyton, D.A. Mankoff, L. Shankar, S.M. Larson, C.C. Sigman, R.L. Schilsky, and D.C. Sullivan, *Progress and promise of FDG-PET imaging for cancer patient management and oncologic drug development.* Clin Cancer Res, 2005. **11**(8): p. 2785-808.
18. Dang, C.V. and G.L. Semenza, *Oncogenic alterations of metabolism.* Trends Biochem Sci, 1999. **24**(2): p. 68-72.
19. Minchenko, O., I. Opentanova, and J. Caro, *Hypoxic regulation of the 6-phosphofructo-2-kinase/fructose-2,6-bisphosphatase gene family (PFKFB-1-4) expression in vivo.* FEBS Lett, 2003. **554**(3): p. 264-70.
20. Semenza, G.L., *HIF-1: mediator of physiological and pathophysiological responses to hypoxia.* J Appl Physiol, 2000. **88**(4): p. 1474-80.

21. Guppy, M., P. Leedman, X. Zu, and V. Russell, *Contribution by different fuels and metabolic pathways to the total ATP turnover of proliferating MCF-7 breast cancer cells.* Biochem J, 2002. **364**(Pt 1): p. 309-15.
22. Wilson, J.E., *Isozymes of mammalian hexokinase: structure, subcellular localization and metabolic function.* J Exp Biol, 2003. **206**(Pt 12): p. 2049-57.
23. Pedersen, P.L., S. Mathupala, A. Rempel, J.F. Geschwind, and Y.H. Ko, *Mitochondrial bound type II hexokinase: a key player in the growth and survival of many cancers and an ideal prospect for therapeutic intervention.* Biochim Biophys Acta, 2002. **1555**(1-3): p. 14-20.
24. Beutner, G., A. Ruck, B. Riede, W. Welte, and D. Brdiczka, *Complexes between kinases, mitochondrial porin and adenylate translocator in rat brain resemble the permeability transition pore.* FEBS Lett, 1996. **396**(2-3): p. 189-95.
25. Shimizu, S., T. Ide, T. Yanagida, and Y. Tsujimoto, *Electrophysiological study of a novel large pore formed by Bax and the voltage-dependent anion channel that is permeable to cytochrome c.* J Biol Chem, 2000. **275**(16): p. 12321-5.
26. Medina, R.A. and G.I. Owen, *Glucose transporters: expression, regulation and cancer.* Biol Res, 2002. **35**(1): p. 9-26.
27. Lane, R.H., S.E. Crawford, A.S. Flozak, and R.A. Simmons, *Localization and quantification of glucose transporters in liver of growth-retarded fetal and neonatal rats.* Am J Physiol, 1999. **276**(1 Pt 1): p. E135-42.
28. Olayioye, M.A., R.M. Neve, H.A. Lane, and N.E. Hynes, *The ErbB signaling network: receptor heterodimerization in development and cancer.* EMBO J, 2000. **19**(13): p. 3159-67.
29. Harari, D., E. Tzahar, J. Romano, M. Shelly, J.H. Pierce, G.C. Andrews, and Y. Yarden, *Neuregulin-4: a novel growth factor that acts through the ErbB-4 receptor tyrosine kinase.* Oncogene, 1999. **18**(17): p. 2681-9.
30. Normanno, N., C. Bianco, L. Strizzi, M. Mancino, M.R. Maiello, A. De Luca, F. Caponigro, and D.S. Salomon, *The ErbB receptors and their ligands in cancer: an overview.* Curr Drug Targets, 2005. **6**(3): p. 243-57.
31. Muthuswamy, S.K., M. Gilman, and J.S. Brugge, *Controlled dimerization of ErbB receptors provides evidence for differential signaling by homo- and heterodimers.* Mol Cell Biol, 1999. **19**(10): p. 6845-57.
32. Henson, E.S. and S.B. Gibson, *Surviving cell death through epidermal growth factor (EGF) signal transduction pathways: implications for cancer therapy.* Cell Signal, 2006. **18**(12): p. 2089-97.
33. Elstrom, R.L., D.E. Bauer, M. Buzzai, R. Karnauskas, M.H. Harris, D.R. Plas, H. Zhuang, R.M. Cinalli, A. Alavi, C.M. Rudin, and C.B. Thompson, *Akt stimulates aerobic glycolysis in cancer cells.* Cancer Res, 2004. **64**(11): p. 3892-9.
34. Downward, J., *Mechanisms and consequences of activation of protein kinase B/Akt.* Curr Opin Cell Biol, 1998. **10**(2): p. 262-7.
35. Marte, B.M. and J. Downward, *PKB/Akt: connecting phosphoinositide 3-kinase to cell survival and beyond.* Trends Biochem Sci, 1997. **22**(9): p. 355-8.
36. Plas, D.R. and C.B. Thompson, *Akt-dependent transformation: there is more to growth than just surviving.* Oncogene, 2005. **24**(50): p. 7435-42.
37. Brazil, D.P. and B.A. Hemmings, *Ten years of protein kinase B signalling: a hard Akt to follow.* Trends Biochem Sci, 2001. **26**(11): p. 657-64.
38. Hahn-Windgassen, A., V. Nogueira, C.C. Chen, J.E. Skeen, N. Sonenberg, and N. Hay, *Akt activates the mammalian target of rapamycin by regulating cellular ATP level and AMPK activity.* J Biol Chem, 2005. **280**(37): p. 32081-9.

39. Vanhaesebroeck, B., S.J. Leevers, K. Ahmadi, J. Timms, R. Katso, P.C. Driscoll, R. Woscholski, P.J. Parker, and M.D. Waterfield, *Synthesis and function of 3-phosphorylated inositol lipids.* Annu Rev Biochem, 2001. **70**: p. 535-602.
40. Manning, B.D. and L.C. Cantley, *AKT/PKB signaling: navigating downstream.* Cell, 2007. **129**(7): p. 1261-74.
41. Sarbassov, D.D., D.A. Guertin, S.M. Ali, and D.M. Sabatini, *Phosphorylation and regulation of Akt/PKB by the rictor-mTOR complex.* Science, 2005. **307**(5712): p. 1098-101.
42. Nyakern, M., P.L. Tazzari, C. Finelli, C. Bosi, M.Y. Follo, T. Grafone, P.P. Piccaluga, G. Martinelli, L. Cocco, and A.M. Martelli, *Frequent elevation of Akt kinase phosphorylation in blood marrow and peripheral blood mononuclear cells from high-risk myelodysplastic syndrome patients.* Leukemia, 2006. **20**(2): p. 230-8.
43. Maira, S.M., I. Galetic, D.P. Brazil, S. Kaech, E. Ingley, M. Thelen, and B.A. Hemmings, *Carboxyl-terminal modulator protein (CTMP), a negative regulator of PKB/Akt and v-Akt at the plasma membrane.* Science, 2001. **294**(5541): p. 374-80.
44. Okoshi, R., T. Ozaki, H. Yamamoto, K. Ando, N. Koida, S. Ono, T. Koda, T. Kamijo, A. Nakagawara, and H. Kizaki, *Activation of AMP-activated protein kinase induces p53-dependent apoptotic cell death in response to energetic stress.* J Biol Chem, 2008. **283**(7): p. 3979-87.
45. Carling, D., *The AMP-activated protein kinase cascade--a unifying system for energy control.* Trends Biochem Sci, 2004. **29**(1): p. 18-24.
46. Costello, K.K.S.a.L.C., *Mitochondria and Cancer*, ed. S. Science. 2009.
47. Shaw, R.J., *Glucose metabolism and cancer.* Curr Opin Cell Biol, 2006. **18**(6): p. 598-608.
48. Cheng, S.W., L.G. Fryer, D. Carling, and P.R. Shepherd, *Thr2446 is a novel mammalian target of rapamycin (mTOR) phosphorylation site regulated by nutrient status.* J Biol Chem, 2004. **279**(16): p. 15719-22.
49. Prives, C. and P.A. Hall, *The p53 pathway.* J Pathol, 1999. **187**(1): p. 112-26.
50. Mathupala, S.P., C. Heese, and P.L. Pedersen, *Glucose catabolism in cancer cells. The type II hexokinase promoter contains functionally active response elements for the tumor suppressor p53.* J Biol Chem, 1997. **272**(36): p. 22776-80.
51. Kondoh, H., M.E. Lleonart, J. Gil, J. Wang, P. Degan, G. Peters, D. Martinez, A. Carnero, and D. Beach, *Glycolytic enzymes can modulate cellular life span.* Cancer Res, 2005. **65**(1): p. 177-85.
52. Bensaad, K., A. Tsuruta, M.A. Selak, M.N. Vidal, K. Nakano, R. Bartrons, E. Gottlieb, and K.H. Vousden, *TIGAR, a p53-inducible regulator of glycolysis and apoptosis.* Cell, 2006. **126**(1): p. 107-20.
53. Okamura, S., C.C. Ng, K. Koyama, Y. Takei, H. Arakawa, M. Monden, and Y. Nakamura, *Identification of seven genes regulated by wild-type p53 in a colon cancer cell line carrying a well-controlled wild-type p53 expression system.* Oncol Res, 1999. **11**(6): p. 281-5.
54. Schwartzenberg-Bar-Yoseph, F., M. Armoni, and E. Karnieli, *The tumor suppressor p53 down-regulates glucose transporters GLUT1 and GLUT4 gene expression.* Cancer Res, 2004. **64**(7): p. 2627-33.
55. Johnson, G.L., H.G. Dohlman, and L.M. Graves, *MAPK kinase kinases (MKKKs) as a target class for small-molecule inhibition to modulate signaling networks and gene expression.* Curr Opin Chem Biol, 2005. **9**(3): p. 325-31.
56. Leaman, D.W., S. Pisharody, T.W. Flickinger, M.A. Commane, J. Schlessinger, I.M. Kerr, D.E. Levy, and G.R. Stark, *Roles of JAKs in activation of STATs and stimulation*

of c-fos gene expression by epidermal growth factor. Mol Cell Biol, 1996. **16**(1): p. 369-75.
57. Mischel, P.S. and T.F. Cloughesy, *Targeted molecular therapy of GBM.* Brain Pathol, 2003. **13**(1): p. 52-61.
58. Kleihues, P. and L.H. Sobin, *World Health Organization classification of tumors.* Cancer, 2000. **88**(12): p. 2887.
59. Pelloski, C.E., K.V. Ballman, A.F. Furth, L. Zhang, E. Lin, E.P. Sulman, K. Bhat, J.M. McDonald, W.K. Yung, H. Colman, S.Y. Woo, A.B. Heimberger, D. Suki, M.D. Prados, S.M. Chang, F.G. Barker, 2nd, J.C. Buckner, C.D. James, and K. Aldape, *Epidermal growth factor receptor variant III status defines clinically distinct subtypes of glioblastoma.* J Clin Oncol, 2007. **25**(16): p. 2288-94.
60. Antonyak, M.A., D.K. Moscatello, and A.J. Wong, *Constitutive activation of c-Jun N-terminal kinase by a mutant epidermal growth factor receptor.* J Biol Chem, 1998. **273**(5): p. 2817-22.
61. Moscatello, D.K., M. Holgado-Madruga, D.R. Emlet, R.B. Montgomery, and A.J. Wong, *Constitutive activation of phosphatidylinositol 3-kinase by a naturally occurring mutant epidermal growth factor receptor.* J Biol Chem, 1998. **273**(1): p. 200-6.
62. Todaro, G.J. and H. Green, *Quantitative studies of the growth of mouse embryo cells in culture and their development into established lines.* J Cell Biol, 1963. **17**: p. 299-313.
63. Ryan, J.A., *Cryogenic Preservation and Storage of Animal Cells*. 2006.
64. He, L. and M.H. Fox, *Comparison of flow cytometry and western blotting to measure Hsp70.* Cytometry, 1996. **25**(3): p. 280-6.
65. Tsuji, A.B., H. Sudo, A. Sugyo, M. Otsuki, M. Miyagishi, K. Taira, T. Imai, and Y.N. Harada, *A fast, simple method for screening radiation susceptibility genes by RNA interference.* Biochem Biophys Res Commun, 2005. **333**(4): p. 1370-7.
66. Tronstad, K.J., K. Berge, E.N. Flindt, K. Kristiansen, and R.K. Berge, *Optimization of methods and treatment conditions for studying effects of fatty acids on cell growth.* Lipids, 2001. **36**(3): p. 305-13.
67. Isobe, I., K. Yanagisawa, and M. Michikawa, *3-(4,5-Dimethylthiazol-2-yl)-2,5-diphenyltetrazolium bromide (MTT) causes Akt phosphorylation and morphological changes in intracellular organellae in cultured rat astrocytes.* J Neurochem, 2001. **77**(1): p. 274-80.
68. Gonzalez, R.J. and J.B. Tarloff, *Evaluation of hepatic subcellular fractions for Alamar blue and MTT reductase activity.* Toxicol In Vitro, 2001. **15**(3): p. 257-9.
69. Berridge, M.V. and A.S. Tan, *Characterization of the cellular reduction of 3-(4,5-dimethylthiazol-2-yl)-2,5-diphenyltetrazolium bromide (MTT): subcellular localization, substrate dependence, and involvement of mitochondrial electron transport in MTT reduction.* Arch Biochem Biophys, 1993. **303**(2): p. 474-82.
70. Bernas, T. and J. Dobrucki, *Mitochondrial and nonmitochondrial reduction of MTT: interaction of MTT with TMRE, JC-1, and NAO mitochondrial fluorescent probes.* Cytometry, 2002. **47**(4): p. 236-42.
71. O'Brien, J., I. Wilson, T. Orton, and F. Pognan, *Investigation of the Alamar Blue (resazurin) fluorescent dye for the assessment of mammalian cell cytotoxicity.* Eur J Biochem, 2000. **267**(17): p. 5421-6.
72. Acin-Perez, R., E. Salazar, M. Kamenetsky, J. Buck, L.R. Levin, and G. Manfredi, *Cyclic AMP produced inside mitochondria regulates oxidative phosphorylation.* Cell Metab, 2009. **9**(3): p. 265-76.

73. Zhong, D., X. Liu, K. Schafer-Hales, A.I. Marcus, F.R. Khuri, S.Y. Sun, and W. Zhou, *2-Deoxyglucose induces Akt phosphorylation via a mechanism independent of LKB1/AMP-activated protein kinase signaling activation or glycolysis inhibition.* Mol Cancer Ther, 2008. **7**(4): p. 809-17.
74. Rossignol, R., R. Gilkerson, R. Aggeler, K. Yamagata, S.J. Remington, and R.A. Capaldi, *Energy substrate modulates mitochondrial structure and oxidative capacity in cancer cells.* Cancer Res, 2004. **64**(3): p. 985-93.
75. Kroemer, G. and J. Pouyssegur, *Tumor cell metabolism: cancer's Achilles' heel.* Cancer Cell, 2008. **13**(6): p. 472-82.
76. Sok, J.C., F.M. Coppelli, S.M. Thomas, M.N. Lango, S. Xi, J.L. Hunt, M.L. Freilino, M.W. Graner, C.J. Wikstrand, D.D. Bigner, W.E. Gooding, F.B. Furnari, and J.R. Grandis, *Mutant epidermal growth factor receptor (EGFRvIII) contributes to head and neck cancer growth and resistance to EGFR targeting.* Clin Cancer Res, 2006. **12**(17): p. 5064-73.
77. Kunkel, M., T.E. Reichert, P. Benz, H.A. Lehr, J.H. Jeong, S. Wieand, P. Bartenstein, W. Wagner, and T.L. Whiteside, *Overexpression of Glut-1 and increased glucose metabolism in tumors are associated with a poor prognosis in patients with oral squamous cell carcinoma.* Cancer, 2003. **97**(4): p. 1015-24.
78. Medeiros, D.M., *Assessing mitochondria biogenesis.* Methods, 2008. **46**(4): p. 288-94.
79. Hansson, A., N. Hance, E. Dufour, A. Rantanen, K. Hultenby, D.A. Clayton, R. Wibom, and N.G. Larsson, *A switch in metabolism precedes increased mitochondrial biogenesis in respiratory chain-deficient mouse hearts.* Proc Natl Acad Sci U S A, 2004. **101**(9): p. 3136-41.
80. Emerit, I., *Reactive oxygen species, chromosome mutation, and cancer: possible role of clastogenic factors in carcinogenesis.* Free Radic Biol Med, 1994. **16**(1): p. 99-109.
81. Kim, I., S. Rodriguez-Enriquez, and J.J. Lemasters, *Selective degradation of mitochondria by mitophagy.* Arch Biochem Biophys, 2007. **462**(2): p. 245-53.
82. D'Autreaux, B. and M.B. Toledano, *ROS as signalling molecules: mechanisms that generate specificity in ROS homeostasis.* Nat Rev Mol Cell Biol, 2007. **8**(10): p. 813-24.
83. Xi, Q., S.Y. Cheranov, and J.H. Jaggar, *Mitochondria-derived reactive oxygen species dilate cerebral arteries by activating Ca2+ sparks.* Circ Res, 2005. **97**(4): p. 354-62.
84. Bonnet, S., S.L. Archer, J. Allalunis-Turner, A. Haromy, C. Beaulieu, R. Thompson, C.T. Lee, G.D. Lopaschuk, L. Puttagunta, G. Harry, K. Hashimoto, C.J. Porter, M.A. Andrade, B. Thebaud, and E.D. Michelakis, *A mitochondria-K+ channel axis is suppressed in cancer and its normalization promotes apoptosis and inhibits cancer growth.* Cancer Cell, 2007. **11**(1): p. 37-51.
85. Jiang, W., Z. Zhu, and H.J. Thompson, *Modulation of the activities of AMP-activated protein kinase, protein kinase B, and mammalian target of rapamycin by limiting energy availability with 2-deoxyglucose.* Mol Carcinog, 2008. **47**(8): p. 616-28.
86. Inoue, A., S. Muranaka, H. Fujita, T. Kanno, H. Tamai, and K. Utsumi, *Molecular mechanism of diclofenac-induced apoptosis of promyelocytic leukemia: dependency on reactive oxygen species, Akt, Bid, cytochrome and caspase pathway.* Free Radic Biol Med, 2004. **37**(8): p. 1290-9.
87. Kim, W.H., J.W. Lee, Y.H. Suh, H.J. Lee, S.H. Lee, Y.K. Oh, B. Gao, and M.H. Jung, *AICAR potentiates ROS production induced by chronic high glucose: roles of AMPK in pancreatic beta-cell apoptosis.* Cell Signal, 2007. **19**(4): p. 791-805.
88. Pedersen, M.W., M. Meltorn, L. Damstrup, and H.S. Poulsen, *The type III epidermal growth factor receptor mutation. Biological significance and potential target for anti-cancer therapy.* Ann Oncol, 2001. **12**(6): p. 745-60.

12. APPENDIX

12.1 Standard curve for protein determination used for western blotting

A number of protein standards (BSA) with a protein content ranging from 0-2000µg/ml were made. The procedure was carried out as previously described in section 7.8.1. Two parallels were made for each sample and the mean value was used to draw a protein standard curve. Absorbance measurements were carried out at 563nm using an UVM340 ELISA reader.

Protein standard (µg/ml)	Absorbance parallel 1	Absorbance parallel 2	Mean	Mean – background (*)
(*) 0	0,189	0,189	0,19	0
25	0,212	0,213	0,21	0,02
125	0,34	0,351	0,35	0,16
250	0,481	0,475	0,48	0,29
500	0,72	0,716	0,72	0,53
750	1,023	1,069	1,05	0,86
1000	1,328	1,301	1,31	1,13
1500	1,761	1,728	1,74	1,56
2000	1,963	2,029	2,00	1,81

Table 12.1 Determination of protein content

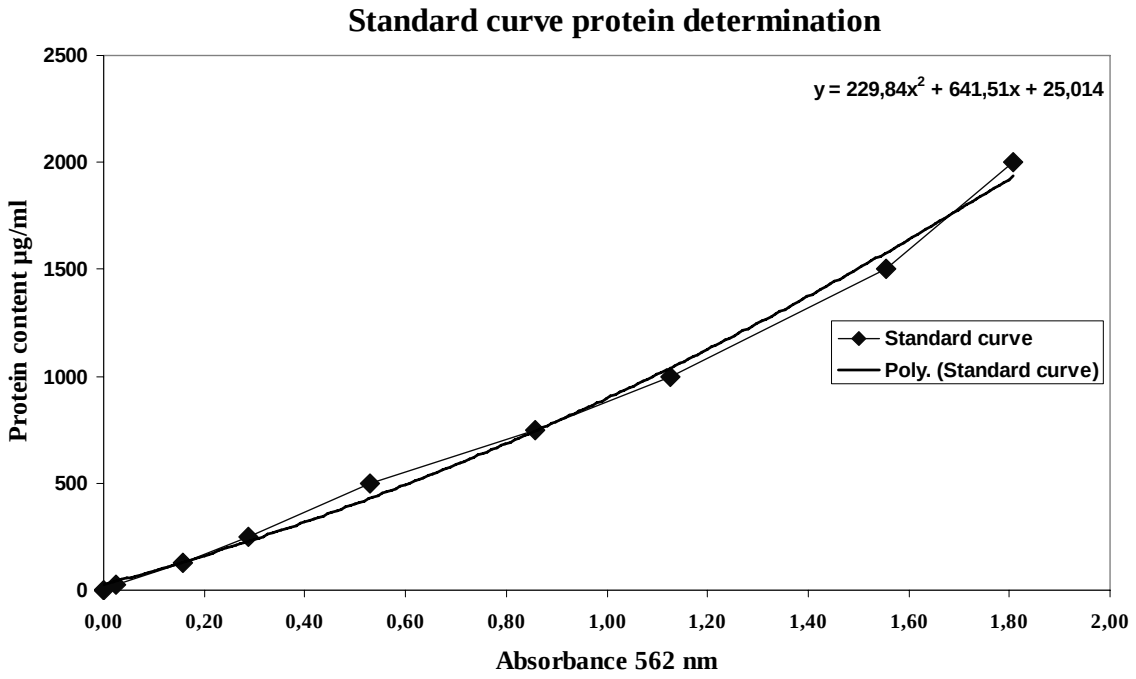

Figure 12.1 Standard curve for protein determination used for western blotting

From the standard curve the equation: y = *229.84x2 + 641.51 + 25.014* was calculated. We used the equation to determine the protein content within our samples.

	Samples	Samples - background	*y = 229.84x2 + 641.51 + 25.014*	Dilution	Protein content (mg/ml)	Mean Protein content (mg/ml)
WT	2,211	2,02	2566,97	1	2,57	**2,57(*)**
	2,217	2,03	2576,93	1	2,58	
	2,029	1,84	2272,85	2	4,55	**4,49**
	1,996	1,81	2221,15	2	4,44	
	1,308	1,12	1257,33	5	6,29	**6,39**
	1,34	1,15	1297,34	5	6,49	
	0,853	0,66	739,46	10	7,39	**7,17**
	0,81	0,62	695,44	10	6,95	
	0,534	0,35	433,12	20	8,66	**8,83**
	0,553	0,36	450,06	20	9,00	
EGFR	2,075	1,89	2345,75	1	2,35	**2,35(*)**
	2,075	1,89	2345,75	1	2,35	
	1,57	1,38	1598,72	2	3,20	**3,19**
	1,568	1,38	1595,99	2	3,19	
	0,946	0,76	837,57	5	4,19	**4,10**
	0,914	0,73	803,36	5	4,02	
	0,601	0,41	493,58	10	4,94	**4,84**
	0,58	0,39	474,41	10	4,74	
	0,328	0,14	260,16	20	5,20	**5,30**
	0,34	0,15	269,70	20	5,39	

Table 12.2 Determination of protein content in U87 glioma cells. (*) concentrations used for further analysis.

12.2 Standard curve for lactate measurements in untreated cells

5 lactate standards with the concentrations 4mM, 3mM, 2mM, 1mM and 0,5mM were made and the procedure was carried out as previously described in section 7.5. Two parallels of each sample were plated and measured using an UVM340 ELISA reader. The mean absorbance of the two parallels was used to make the lactate standard curve. (The plated samples were measured twice – before and after addition of LDH. The absorbances from the first measurement were subtracted from the second measurement, and these calculations are not shown.)

Lactate standard (mM)	Absorbance parallel 1	Absorbance parallel 2	Mean	Mean – background (*)
(*) 0	0,300	0,352	0,326	0
0,5	0,397	0,425	0,411	0,085
1	0,464	0,497	0,481	0,155
2	0,542	0,598	0,570	0,244
3	0,732	0,770	0,751	0,425
4	0,846	0,830	0,838	0,512

Table 12.3 Absorbance determination of lactate standards

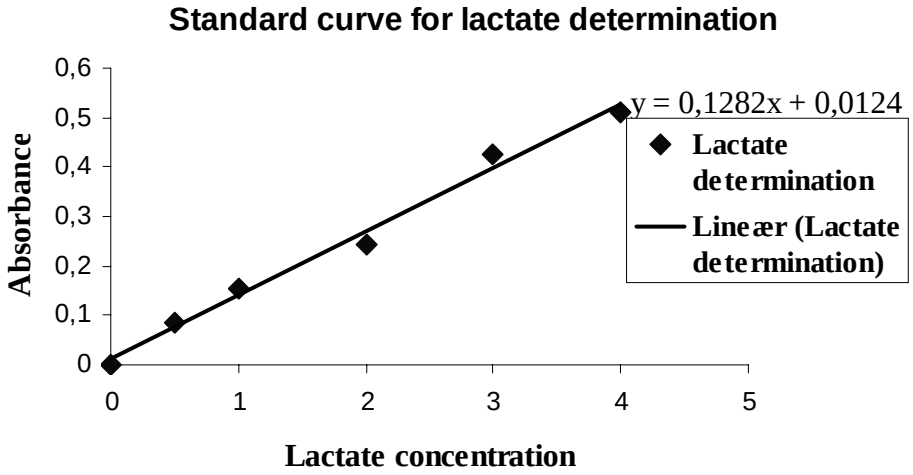

Figure 12.2 Standard curve for lactate determination in untreated cells

The experiment was carried out using culture medium from two distinct dates, hence Run 1 and Run 2.

Run 1		Run 2	
Cell type	**Cell number**	**Cell type**	**Cell number**
EGFR vIII	$1.17x10^6$ cells/ml	EGFR vIII	$0.54x10^6$ cells/ml
WT	$1.05x10^6$ cells/ml	WT	$0.47x10^6$ cells/ml

Table 12.4 Cell number in the culture the medium was tapped from

From the standard curve (Figure 12.2) the equation: y = *0,1282x + 0,0124* was calculated. We used the equation to determine the lactate concentration within our samples.

	Absorbance parallel 1	Absorbance parallel 2	Mean absorbance	y = 0.1282x+0.0124	Dilution	mM Lactate	Mean lactate concentration
EGFR vIII Run 1	2,808	2,884	*2,52*	19,56	**1**	19,56	**50,17mM**
	2,485	2,646	*2,2395*	17,37	**2**	34,74	
	1,598	1,513	*1,2295*	9,49	**5**	47,47	
	1,032	0,873	*0,6265*	4,79	**10**	47,90	
	0,689	0,793	*0,415*	3,14	**20**	62,81	
	0,588	0,344	*0,14*	1,00	**40**	39,81	
WT Run 1	2,755	2,889	*2,496*	19,37	**1**	19,37	**38,47mM**
	2,169	2,241	*1,879*	14,56	**2**	29,12	
	1,179	1,196	*0,8615*	6,62	**5**	33,12	
	0,726	0,814	*0,444*	3,37	**10**	33,67	
	0,543	0,694	*0,2925*	2,18	**20**	43,70	
	0,498	0,457	*0,1515*	1,09	**40**	43,40	
EGFR vIII Run 2	2,418	2,313	*2,0395*	15,81	**1**	15,81	**21,69mM**
	1,045	0,765	*0,579*	4,42	**2**	8,84	
	0,805	0,806	*0,4795*	3,64	**5**	18,22	
	0,609	0,599	*0,278*	2,07	**10**	20,71	
	0,519	0,493	*0,18*	1,31	**20**	26,15	
	0,402	0,417	*0,0835*	0,55	**40**	22,18	
WT Run 2	1,93	1,681	*1,4795*	11,44	**1**	11,44	**13,19mM**
	0,871	0,959	*0,589*	4,50	**2**	8,99	
	0,721	0,703	*0,386*	2,91	**5**	14,57	
	0,558	0,529	*0,2175*	1,60	**10**	16,00	
	0,445	0,354	*0,0735*	0,48	**20**	9,53	
	0,389	0,379	*0,058*	0,36	**40**	14,23	

Table 12.5 Determination of lactate secretion within untreated glioma cells. The mean of the lactate values presented in light grey were used to determine the lactate concentration within the used culture media.

12.2 Standard curve for lactate measurements in treated cells

As for the lactate measurements for untreated cells, 5 lactate standards with the concentrations 4mM, 3mM, 2mM, 1mM and 0,5mM were made and the procedure was carried out as previously described in section 7.5. Two parallels of each sample were plated and measured using an UVM340 ELISA reader. The mean absorbance of the two parallels was used to draw the lactate standard curve. Here a standard curve was made for each of the cell lines. (The plated samples were measured twice – before and after addition of LDH. The absorbance's from the first measurement were subtracted from the second measurement, and these calculations are not shown.)

Lactate standard (mM)	Absorbance parallel 1	Absorbance parallel 2	Mean	Mean – background (*)
(*) 0	0,34	0,37	0,36	0,000
0,5	0,41	0,45	0,43	0,073
1	0,50	0,53	0,51	0,158
2	0,62	0,70	0,66	0,304
3	0,79	0,86	0,82	0,466
4	0,84	0,93	0,89	0,530

Table 12.6 Absorbance determination of WT lactate standards

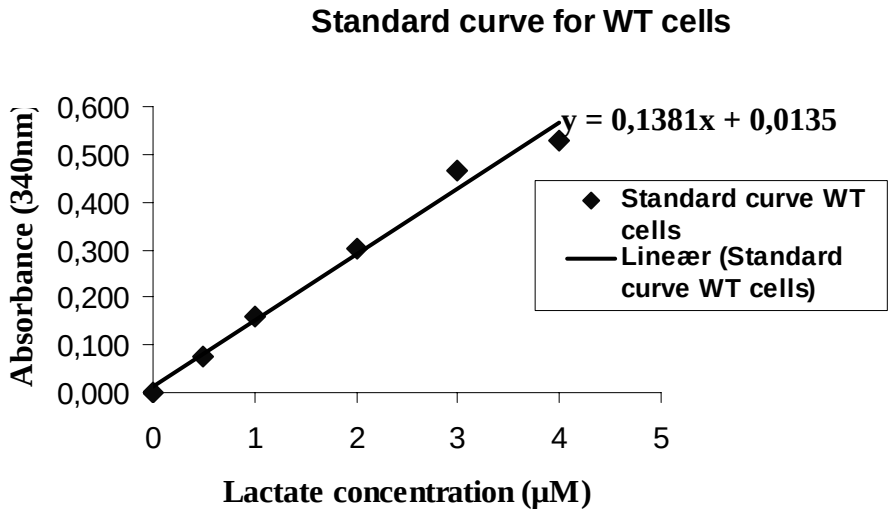

12.3 Standard curve for lactate determination in treated WT cells

Lactate standard (mM)	Absorbance parallel 1	Absorbance parallel 2	Mean	Mean – background (*)
(*) 0	0,33	*0,38*	*0,36*	0,00
0,5	0,40	*0,43*	*0,41*	0,06
1	0,45	*0,49*	*0,47*	0,11
2	0,60	*0,66*	*0,63*	0,27
3	0,62	*0,75*	*0,69*	0,33
4	0,78	*0,83*	*0,81*	0,45

Table 12.7 Absorbance determination of EGFR vIII lactate standards

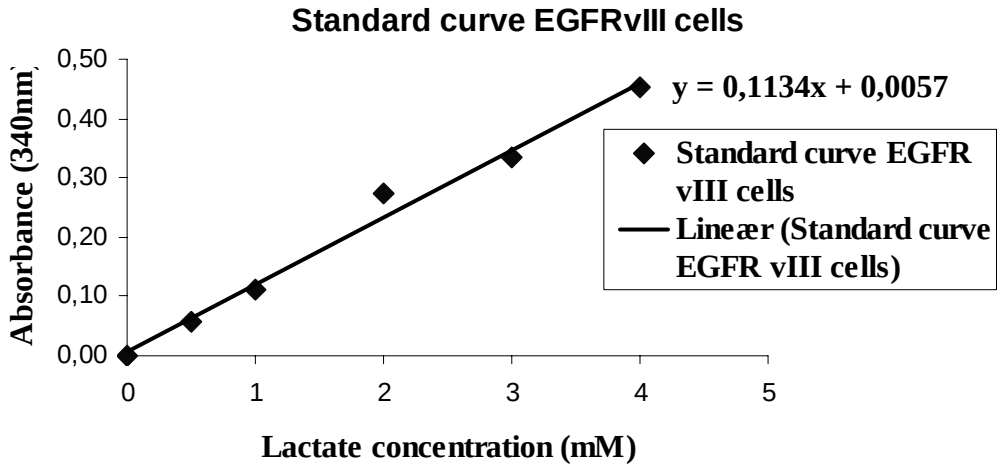

12.4 Standard curve for lactate determination in treated EGFR vIII cells

From the standard curves (Figure 12.3 and 12.4) the equations; y = 0.1381x + 0.0135 (WT) and y = 0.1134x + 0.0057 (EGFR vIII) were calculated. We used the equations to determine the lactate concentrations within our samples.

	Mean absorbance Parallel 1 and 2	Equation (*)	Dilution	mM Lactate
WT control	0,338	2,351		**47,02**
WT 2DG 0.5µM	0,370	2,580		**51,61**
WT 2DG 1µM	0,328	2,279	20	**45,57**
WT rotenone 500nM	0,496	3,495		**69,90**
WT rotenone 0.1µM	0,449	3,150		**63,00**
WT control	0,291	2,006		**80,23**
WT 2DG 0.5µM	0,261	1,789		**71,54**
WT 2DG 1µM	0,295	2,035	40	**81,39**
WT rotenone 500nM	0,418	2,930		**117,21**
WT rotenone 0.1µM	0,384	2,682		**107,27**
EGFR vIII control	0,372	3,233		**64,66**
EGFR vIII 2DG 0.5µM	0,307	2,657		**53,14**
EGFR vIII 2DG 1µM	0,327	2,830	20	**56,61**
EGFR vIII rotenone 500nM	0,429	3,730		**74,60**
EGFR vIII rotenone 0.1µM	0,465	4,053		**81,06**
EGFR vIII control	0,317	2,742		**109,69**
EGFR vIII 2DG 0.5µM	0,296	2,557		**102,28**
EGFR vIII 2DG 1µM	0,261	2,251	40	**90,05**
EGFR vIII rotenone 500nM	0,357	3,101		**124,03**
EGFR vIII rotenone 0.1µM	0,378	3,280		**131,21**

Table 12.8 Determination of lactate secretion within treated glioma cells. (*) For WT cells the equation "y = 0.1381x + 0.0135" were used, while for EGFR vIII cells the equation "y = 0.1134x + 0.0057" were used.

The same number of cells was plated before treatment with 2DG/rotenone and measurement of the lactate secretion.